NASA TECHNICAL NOTE

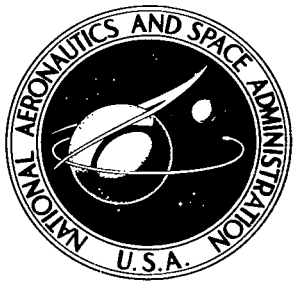

NASA TN D-8116

NASA TN D-8116

DENSE PLASMA FOCUS PRODUCTION IN A HYPOCYCLOIDAL PINCH

Ja H. Lee, Donald R. McFarland, and Frank Hohl

Langley Research Center
Hampton, Va. 23665

NATIONAL AERONAUTICS AND SPACE ADMINISTRATION • WASHINGTON, D. C. • DECEMBER 1975

1. Report No.	2. Government Accession No.	3. Recipient's Catalog No.
NASA TN D-8116		

4. Title and Subtitle	5. Report Date
DENSE PLASMA FOCUS PRODUCTION IN A HYPOCYCLOIDAL PINCH	December 1975
	6. Performing Organization Code

7. Author(s)	8. Performing Organization Report No.
Ja H. Lee, Donald R. McFarland, and Frank Hohl	L-10549
	10. Work Unit No.
9. Performing Organization Name and Address	506-25-31-01
NASA Langley Research Center Hampton, Va. 23665	11. Contract or Grant No.
	13. Type of Report and Period Covered
12. Sponsoring Agency Name and Address	Technical Note
National Aeronautics and Space Administration Washington, D.C. 20546	14. Sponsoring Agency Code

15. Supplementary Notes

Ja H. Lee: Vanderbilt University, Nashville, Tennessee
Donald R. McFarland: Langley Research Center
Frank Hohl: Langley Research Center

16. Abstract

A new type of high-power pinch apparatus consisting of disk electrodes was developed and diagnostic measurements to study its mechanism of dense plasma production have been made. The collapse fronts of the current sheets are well organized and dense plasma focuses are produced on the axis with radial stability in excess of 5 μs. A plasma density greater than 10^{18} cm^{-3} is determined with Stark broadening and CO_2 laser absorption. A plasma temperature of $\approx$1 keV is measured with differential transmission of soft X-rays through thin foils. Essentially complete absorption of a high-energy CO_2 laser beam has been observed. The advantages of this apparatus over the coaxial plasma focus are in (1) the plasma volume, (2) the stability, (3) the containment time, (4) the easy access to additional heating by laser or electron beams and, (5) the possibility of scaling up to a multiple array for high-power operation.

17. Key Words (Suggested by Author(s))		18. Distribution Statement
Thermonuclear fusion	X-ray emission	Unclassified – Unlimited
Dense plasma	Dense plasma focus	
Laser plasma interaction	Spindle focus	
Plasma containment	Hypocycloidal pinch	Subject Category 75

19. Security Classif. (of this report)	20. Security Classif. (of this page)	21. No. of Pages	22. Price*
Unclassified	Unclassified	42	$3.75

*For sale by the National Technical Information Service, Springfield, Virginia 22161

DENSE PLASMA FOCUS PRODUCTION IN A HYPOCYCLOIDAL PINCH

Ja H. Lee,* Donald R. McFarland, and Frank Hohl
Langley Research Center

SUMMARY

A new type of high-power pinch apparatus consisting of disk electrodes was developed and diagnostic measurements to study the mechanism of dense plasma production have been made. The collapse fronts of the current sheets are well organized and dense plasma focuses are produced on the axis with radial stability in excess of 5 μs. A plasma density greater than 10^{18} cm^{-3} is determined with Stark broadening and CO_2 laser absorption. Essentially complete absorption of a high-energy CO_2 laser beam has been observed. A plasma temperature of $\approx$1 keV is measured with differential transmission of soft X-rays through thin foils. The advantages of this apparatus over the coaxial plasma focus are in (1) the plasma volume, (2) the stability, (3) the containment time, (4) the easy access to additional heating by laser or electron beams, and (5) the possibility of scaling up to a multiple array for high-power operation.

INTRODUCTION

The dense plasma focus is presently the most successful plasma device in approaching Lawson's criterion for a thermonuclear fusion reactor. It has been demonstrated that nuclear fusion reaction rates in a plasma focus can be as high as 10^{19}/s in deuterium, and 10^{21}/s in deuterium-tritium mixture. (See refs. 1 to 5.) The scaling law for the dense plasma focus apparatus has been established experimentally up to several hundred kJ input energy, and a break-even point at 10 MJ has been predicted theoretically. (See ref. 6.) However, because of its obvious geometrical limitations, it is difficult to foresee development of a large-scale reactor from its present form.

Attempts to couple two plasma focuses have been unsuccessful for both Mather and Filippov types. (See refs. 7 and 8.) Mather in 1965 (ref. 7) tested the idea of combining a two-gun system in opposite polarity in order to superimpose the two high-density plasma focuses. It was anticipated that a large axial current stream would connect the two opposite-polarity center electrodes when the current sheet collapsed to the axis; and, as a result, the confinement time would be longer and there would be further heating of the plasma. However, the experiment showed sharply reduced neutron production when

*Vanderbilt University, Nashville, Tennessee.

two guns were simultaneously operated. This result was attributed to the formation of predischarges in the guns which interfered with the final current-sheet collapse.

A new type of high-power pinch apparatus consisting of three disk electrodes as a radical improvement over the coaxial types of plasma focus apparatus has been developed. The new apparatus called a hypocycloidal-pinch (or HCP) apparatus is based on the invention disclosed to NASA by Ja H. Lee in early 1970 (NASA W-1418). Preliminary results obtained with this apparatus have been reported elsewhere. (See refs. 9 and 10.) There have been some independent studies on a disk geometry for production of a dense plasma – analytically by Mayer (ref. 11) in 1970 and experimentally by Ware et al. (ref. 12) in 1973. However, these authors had limited their work to preliminary speculations on a fixed design and no results were obtained with a complete geometry as presented here.

The present report describes the geometry and operation of the hypocycloidal-pinch apparatus and presents the results of diagnostic measurements made on a 20-cm-diameter prototype. The advantages of the new hypocycloidal pinch over the coaxial plasma focus devices are also discussed.

SYMBOLS

A	area, m^2
B	magnetic induction, T
C	capacitance, F
c	speed of light, cm/sec
D	photographic density
D_α	α-line of deuterium
D_β	β-line of deuterium
E	voltage, V
E_γ	X-ray energy, eV
F	force, N

f	frequency, Hz
h	interelectrode spacing, m
I	electric current, A; or laser power, W
I_p	peak current of an oscillatory circuit, A
i	detector current, A
J	electric current density, A/m^2
L	inductance of an electric circuit, H
ℓ_{ab}	absorption length, cm
m	mass, kg
n_e	electron number density, cm^{-3}
p	pressure, Pa
R	radius of the device, m; or resistance, Ω
r	radial coordinate, m
S	current responsitivity, A/W
T	dimensionless coordinate, t/T_k
T_e	electron temperature, eV
T_k	$= \left[\dfrac{\pi \rho R^4}{10^{-7} \left(\dfrac{dI}{dt} \right)_{av}^2} \right]^{1/4}$ (see eq. (A3))
$T_{1/4}$	quarter period or rise time, s
t	time, s

V	rundown speed of a current sheet, m/s
x	dimensionless coordinate, r/R
Z	ionic charge number; or impedance, Ω
z	axial coordinate
δ	displacement, m
η	total scattering cross section, I_s/I_o
λ	wavelength, Å
μ_o	magnetic permeability of free space, $4\pi \times 10^{-7}$ H/m
ρ	density, kg/m^3
ω	plasma frequency, Hz

Subscripts:

av	average
e	electron
l	lower chamber
max	maximum
min	minimum
o	initial condition
r	radial
s	total scattered
sd	scattered power entering a detector

u upper chamber

ϕ azimuthal

Abbreviations:

ARB arbitrary

Div. division of time scale on oscillogram

HCP hypocycloidal pinch

IR infrared detector

MHD magnetohydrodynamics

PF coaxial plasma focus

TEA transverse excitation at atmospheric pressure

L-C inductance-capacitance

Arrows over symbols denote vectors.

HYPOCYCLOIDAL-PINCH APPARATUS

Figure 1 shows the cross section of the hypocycloidal-pinch apparatus which consists of two disk cathodes sharing a common disk anode. One can visualize this geometry as formed by the cross section of the coaxial plasma focus apparatus (fig. 2) rotated about an axis situated in front of and perpendicular to the center electrode. The insulators placed between the electrodes are also in the form of a disk and provide an inverse pinch geometry for the initial breakdown currents; thus, one of the important features for the coaxial plasma focus apparatus is retained.

The lower and upper current sheets launched from the insulators advance radially toward the center hole where they collapse and interact with each other. Both disk cathodes are perforated to reduce the mass loading of the current sheet in flight similar to the outer electrode of the regular plasma focus. (See refs. 1 to 5.)

The collapse of current sheets is timed so that the maximum current occurs when the sheets reach the edges of the center hole; as a result, two strong pinches are formed around the axis of the apparatus. These pinches produce a pair of dense plasma focuses, each of which resembles the focused plasma produced in a Filippov-type plasma focus device. However, production of an additional volume of a dense plasma with hypocycloidal boundary is expected as the pinched current sheets fall into the center of the hole. This result is expected since the azimuthal magnetic fluxes behind the current sheets in the upper and lower chambers are antiparallel as shown in figure 3 and a magnetic neutral plane is formed on the midplane of the apparatus. A strong magnetic pressure is exerted on the current sheets and forces the sheets to accelerate in the axial direction toward the midplane of the apparatus. Consequently, a dense plasma is produced with nearly hypocycloidal shape.

Similar to the coaxial plasma focus devices, the following five phases of the discharge occur in the dynamics of the hypocycloidal pinch: (1) the inverse pinch over the insulator at the beginning of the discharge; (2) the rundown of the current sheets as a result of the $\vec{J} \times \vec{B}$ force toward the center hole; (3) the collapse of the current sheets into the center hole; (4) the formation of plasma focuses (and their interaction); and (5) the diffusion and cooling of the plasma.

The prototype used in the experiment has a rundown radius of 10 cm with a 5-cm-diameter center hole. The spacing between the anode and cathode disks is 2.5 cm. Figure 4 is the photograph of the device. It is operated at a filling pressure of 133 to 1330 Pa (1 to 10 torr) of deuterium with a few percent of argon or xenon impurities added to improve X-ray production and diagnostic measurements. The operating procedure of the hypocycloidal-pinch apparatus is similar to that of the coaxial plasma focus. The following sequence is used for each run:

(1) Filling the apparatus with working gas at a desired pressure,

(2) Charging the capacitor bank to the required voltage, and

(3) Firing of the trigatron switches to discharge the stored energy into the HCP apparatus.

The prototype system has the following electrical parameters: capacitance, 150 μF; external inductance, 20 nH; inductance of the prototype, 4 nH; and the current rise time (or a quarter period), 3 μs. The apparatus is energized by a capacitor bank with an energy storage of 27 kJ at 19 kV.

DIAGNOSTIC MEASUREMENTS

Dynamics of the current sheet have been studied for different diameters of the center hole and for different gas pressures. For hole diameters less than 3 cm, no X-ray

production or focus formation was observed. Also, for a center hole with a diameter less than 2.5 cm, nonuniform erosion of the surface of the hole was observed. However, the collapse of the current sheets for a larger (5-cm-diameter) hole is well organized and radial stability of the focused plasma is sustained for several μs. Maximum X-ray production was observed when an initial pressure of 400 Pa (3 torr) was used. Figure 5 shows streak pictures taken through a slit placed across a diameter of the center hole. The strong emission of light from the focused plasma is attenuated through a 4D neutral density filter to prevent overexposure of the film. The objective lens of the camera is covered with a $\lambda = 5600 \pm 10$ Å interferometric filter to allow observation of continuum emission only. The pictures reveal production of a luminous plasma on the axis which has a radial stability for over 5 μs. The diameter of the luminous plasma column is approximately 5 mm and is well centered on the axis of the hole. Note that the diameter of the filter is small enough to insure that it does not cover the edge of the hole. This arrangement allows observation of the hole edge in figure 5. The boundary of the plasma is sharply defined and no MHD instabilities are detectable in the pictures. Figure 6 shows frame pictures of the same event. A still reference picture is also shown. The frame pictures shown were taken in sets of three at a time with different neutral density filters for each set. The filter density was increased as the compression progressed to prevent overexposure. The progress of symmetrical compression is well illustrated. The collapse speed measured from these pictures is 3.3×10^4 m/s. Figure 7 shows the axial motion of the plasma. These pictures were obtained with the optical axis of the image-converter camera oriented to form a 10° angle with the axis of the apparatus. The still reference picture in figure 7(b) shows the field of view of the camera. The streak picture in figure 7(c) shows that there are three stages in the axial motion. First the current sheets collapse to form a 10-cm-long column on the axis with a dense focus at each end. Axial compression then follows, ≈ 2 μs later its length is reduced to ≈ 3 cm, and a fading of visible radiation follows. Lastly, the plasma column splits into two focuses separated by a distance of ≈ 5 cm which is the distance between the central planes of two electrode pairs. However, there are occasions when no axial compression is observed as shown on the streak picture in figure 7(d). The two focuses seem to stay separated for their whole lifetimes.

Figure 8 shows the rundown speed of the current sheet measured on streak pictures taken with an image-converter camera which is focused to a 1-mm-wide slit located along a radius of the discharge chamber. The time history of the advancing luminous front of the current sheet is then obtained from the image-converter pictures and yields the rundown speed. The rundown speed V was measured as a function of the filling pressure p. For the deuterium pressure range from 67 to 2000 Pa (0.5 to 15 torr) it is in agreement with a snowplow model (see appendix A) which predicts $V \propto p^{-1/4}$. (See ref. 13.) These measurements were made with the capacitor bank energy of 27 kJ at 19 kV.

Figure 9 is a time-integrated X-ray pinhole picture taken on the axis of the apparatus. The X-rays come through a 250-μm beryllium foil and 1-mm-diameter pinhole. The picture shows that soft X-ray emission is concentrated in a volume of $\approx$5-mm diameter on the axis and that it is well separated from the wall surrounding the hole. The size of this volume is in agreement with the luminous plasma shown earlier in figure 5.

Figure 10 compares temporal evolution of the voltage, the dI/dt variation at the center electrode, the X-ray emission detected by a fast scintillator-photomultiplier system, and the continuum emission in the visible spectrum. The dense plasma formation in the hypocycloidal-pinch apparatus is characterized by a sharp spike on the voltage and dI/dt signal and simultaneous onsets of strong continuum and X-ray emission, similar to a coaxial plasma focus apparatus. However, the voltage signal from the center electrode (fig. 10(a)) does not show the high-frequency oscillation following the spike which is often observed from the coaxial type. (See refs. 1 to 5.) This result may indicate a lack of fast-growing instabilities in a hypocycloidal-pinch apparatus. Furthermore, the continuum and X-ray emissions are sustained for a period of 5 μs after the current-sheet collapse. This time is more than an order of magnitude larger than that of a coaxial plasma focus. This result is well illustrated in figure 11 which compares the periods of X-ray emission from these two apparatus.

The electron temperature T_e of the plasma is determined by the differential transmission of the X-rays through absorbing foils of different thicknesses. Figure 12 shows the exposed film and densitometer traces of the intensities of the transmitted X-rays observed through 250-, 500-, 750-, and 1000-μm beryllium foils. With the assumption of a Maxwellian distribution, the intensity ratio of the transmitted X-rays can be used to determine the electron temperature of the plasma by making use of calculations by Elton and Anderson (ref. 14) and Elton (ref. 15). For example, after subtracting the gray level of the film, the intensity ratio of the transmitted X-rays through 250-μm and 500-μm foils is 0.55 and indicates that the electron temperature is $\approx$1 keV.

The assumption of a Maxwellian velocity distribution for electrons is considered to be reasonable since the plasma lifetime of $\approx$5 μs is very long compared with the electron thermalization time of the order of 10 ns. Also, the X-rays are detectable through a 1.5-mm-thick aluminum absorber; thus, it is indicated that the high-energy tail extends beyond the 8-keV K-edge of aluminum. However, no X-rays were detectable behind lead foils; therefore, the emission of hard X-rays $\left(E_\gamma > 80 \text{ keV}\right)$ is small. Nevertheless, low-level neutron production has been observed with a scintillation neutron detector even at the comparatively low capacitor bank energy of 27 kJ.

The density of the plasma is estimated by the line broadening of D_α and D_β. (See ref. 16.) Figure 13 shows the image-converter camera-spectrometer system used to observe the time-resolved spectra. A 500-gain image-converter camera is focused

on the exit slit of a 1.5-m spectrometer which had a dispersion of 0.556 nm/mm. Figure 14 shows the time-resolved spectra obtained with this system. A wavelength range of 30 nm is recorded for 50 μs. Since the broadening in a high-density plasma is mainly due to the Stark broadening and since Doppler broadening is negligible, the half-width of the lines can be used as a measure of plasma density. Figure 15 shows the plasma density variation in time obtained by this method. A densitometer is used to obtain the broadened line width. The broadening of the D_α line produced by the first pinch is so wide (>10 nm) that accurate pressure determination cannot be made. However, the broadening indicates that $n_e > 10^{18}$ cm^{-3}, the upper limit of the useful range of this method. This result was expected from the compression ratio of ≈100 estimated with the snowplow model.

The particle confinement time is measured by means of high-power CO_2 laser transmission. Figure 16 shows the experimental setup and the experimental results. A 50-J, TEA CO_2 laser beam with 150-ns pulse width is focused to a diameter of 5 mm by a germanium lens. The beam irradiates the full cross section of the focused plasma in the HCP apparatus. The laser firing time is varied so that the interaction at different times of the plasma life can be determined. The incident and transmitted laser powers were measured with pyroelectric infrared detectors IR 1 and 2, respectively. IR 1 monitors a small fraction of the incident laser power which is reflected by a small mirror. IR 2 has a higher sensitivity than IR 1 and measures the transmitted or scattered laser power.

Figure 16 presents sets of two double-trace oscillograms which record the voltage at the center electrode of the HCP, the incident power of the CO_2 laser by IR 1, transmitted laser power by IR 2 at 180°, and the X-ray emission. Time t is the elapsed time from the onset of X-ray emission to the CO_2 laser firing as monitored by IR 1. Figure 16(a) shows the full transmission of laser radiation before (at $t = -0.2$ μs) the plasma production on the axis. Less than 1-percent transmission is recorded for $t = 0$, 0.5, and 12 μs. (See figs. 16(b), 16(c), and 16(d).) For these times the maximum sensitivity of the scope amplifier is used to verify the results. Figure 16(e) shows that at $t = 72$ μs, there is 30-percent transmission through the cooling and expanding plasma. Note that both IR detectors have a fast rise time (<10 ns) but a long decay time characteristic of pyroelectric sensing elements. Only the leading edge of the pulse is meaningful.

The back and side scattering of the laser power by the plasma has also been investigated. For this purpose, the IR 2 detector is located 10° and 90° with respect to the optical axis as shown in figure 16.

The sensitivity of the IR 2 (KT-1100, Laser Precision Corp.) was 0.125 μA/watt. When this detector is located at a distance of 1 m from the plasma, which is irradiated

by a pulsed laser of 5×10^8 W (or 100 ns pulse of 50 J), the sensitivity of the detector is sufficient to give an observable signal for the total scattered power of as small as 5×10^{-3} times the incident power. (See appendix B.)

The laser firing time t is varied with respect to the onset of the X-ray emission, t = 0, as for the transmission experiment. Since the scattering is expected to increase with the plasma density, the laser firing time t is varied with a small interval of 100 ns between runs so that the scattering from the plasma at the maximum compression can be detected. However, for both 10^o and 90^o directions, no scattered intensity above the detector threshold was observed for the laser firings made in the period $-0.2 < t < 75$ μs. This result indicates the total scattered intensity is less than 1 percent of the incident laser power.

The combined results of the transmission and scattering measurements lead to the conclusion that near complete absorption of the laser energy occurs in the plasma.

The impurity level of the plasma generated in the hypocycloidal pinch was investigated with time-resolved spectrometry. No detectable line emissions expected from wall erosion were observed above the continuum intensity during the first pinch period. The impurity line emissions became apparent only at a later time as expected as shown in figure 17. Figure 18 shows some of the impurity lines which have been identified.

DISCUSSION

The final compression and heating in Z-pinch devices such as the coaxial plasma focus or the hypocycloidal pinch are known to depend on the degree of symmetry that is maintained for the entire flight of the Z-pinch current sheets. In the hypocycloidal-pinch apparatus, the most serious excursion from symmetry may occur when one current sheet moving in the upper or lower chamber gets in front of the other and thereby arrives at the center hole too soon. However, no appreciable delay is observed between the arriving time of the upper and lower current sheets at the center hole. The observations made in the streak mode, as in figure 5, clearly show that the final collapse of the upper and lower current sheets are simultaneous within the framing time of 50 ns. This result is also confirmed by the shape of the X-ray pulses, as shown in figure 10, for which one would expect double peaks corresponding to each collapse of the two current sheets if they occurred at two different times. Indeed, the observations indicate that the geometry of the hypocycloidal-pinch apparatus provides a self-stabilizing effect on current sheet dynamics, as discussed in reference 11. The self-stabilizing effect can be easily understood by considering the advancing current fronts as two parallel circuit elements with time-varying inductance as the load of a common power source. (See fig. 19(a).) The ponderomotive force $\vec{J} \times \vec{B}$ exerted on the current sheet which lags behind and forms a

circuit with a smaller impedance will be stronger than the one that leads and will result in an increase of acceleration to "catch up" to the leading front.

The other common phenomenon undesirable for a Z-pinch is spoking or filamentation of the current sheet. For the hypocycloidal pinch no evidence was found of spoking of the current sheets by means of either the fast camera pictures or the "footprints" of the currents on the electrodes. The main reason for the uniform discharge at the outer periphery may come from the fact that the design of the HCP accommodates the inverse pinch phase, similar to the coaxial plasma focus apparatus. It is known that the initial breakdown in a form of an inverse pinch is important for symmetrical current-sheet formation in a plasma focus apparatus. The inverse pinch is also helpful for reducing impurity level in the plasma since the current sheets will quickly leave from the surface of the insulator. The uniform discharge at the periphery is also a reward of careful construction to maintain a high degree of axial symmetry of the apparatus. It should be mentioned that the output cables from different switches are criss-crossed at the collector plates to insure simultaneous breakdown at all points of the periphery.

The rundown speed of the current sheet of 5×10^4 m/s at 665 Pa (5 torr) is rather low compared with that of the coaxial plasma focus apparatus (3×10^5 m/s). However, this can be understood by taking account of the fact that the stored energy is divided into two chambers of the hypocycloidal pinch (HCP), whereas the coaxial plasma focus apparatus (PF) has only one current sheet to be accelerated. Also in the HCP, the current sheets are radially compressed from the beginning and tend to have a large mass pickup in contrast to the rather low mass pickup in the PF which runs down in an annular space with a constant cross section. Therefore, a larger mass for the focused plasma is expected in the HCP than in the PF and this is indeed confirmed by the measurements of the X-ray emitting volume (≈5-mm diameter for the HCP and ≈1-mm diameter for the PF). The slower rundown speed in the HCP may be the result of the large mass pickup. However, since the snowplow model gives a scaling of the rundown speed with the capacitor bank energy, as shown in appendix A, a higher rundown speed can be obtained easily by increasing the stored energy.

The results obtained with the HCP also show a remarkable improvement in both energy and particle confinement times. The full width of the X-ray pulse extends to 5 μs with a sharp spike at the onset. This is an order of magnitude longer than the corresponding period of X-ray emission in the regular plasma focus apparatus, as shown in figure 11. In fact, the X-ray emission in HCP continues until the end of the first half cycle of its discharge circuit. This condition may indicate that the plasma confinement time in HCP is limited only by the current decay at the second quarter cycle. This result also contrasts to the 150-ns X-ray spike without an extended tail in the spindle focus with a pair of disks observed by Ware et al. (ref. 12). The extended confinement of the plasma in the HCP

seems to result from the interaction of two focuses in the magnetic-neutral plane formed by the cusp configuration of the current sheets in the center hole, which is a unique feature of the HCP. One should also note that the simultaneous arrival of the upper and lower current sheets on the axis of the center hole is necessary to form the symmetric cusp configuration of the current sheets. The excellent radial stability beyond the period of the initial spike observed in the HCP leads one to believe these requirements are fully met and the configuration is well maintained throughout the later period during which the plasma diffuses and expands as the currents oscillate and decay. This interpretation is further justified by the results of the CO_2 laser absorption experiment which indicate prolonged particle trapping near the axis for five periods of the circuit oscillations. Therefore, one could possibly achieve further extension of the containment time of the dense plasma produced at the first pinch by shaping the current wave form to a non-oscillatory mode with a crowbar circuit as is often adopted for the capacitor bank used for a theta pinch.

The self-stabilizing mechanism of the hypocycloidal current sheets discussed earlier may be effective even after the collapse of the current sheets into the hole and, as a result, there is a suppression of the fast-growing MHD modes. The self-stabilization mechanism after the collapse can also be understood by elementary consideration of the circuit induction with a virtual displacement of one of the current sheets. As shown in figure 19(b), displacements from the equilibrium of one of the current sheets tend to reduce the inductance of the circuit to which the current sheet is attached. This condition, in turn, results in a stronger $\vec{J} \times \vec{B}$ force in the direction against the displacement. The force δF on the current displaced by δ is

$$\delta F = -4L_0 \frac{I^2}{R^2} \delta$$

where I is the total current, $L_0 = \mu_0 h/2\pi$, R is the radius of the device, and h is the interelectrode spacing. The negative sign indicates that this force will act to restore the equilibrium. Note also that the restoring force is linear in this analysis. The restoring force resulting from an increase of the $\vec{J} \times \vec{B}$ force can be expressed in a different way. It is the result of the "bunching" of lines of force in the direction of the displacement which leads to an increase in magnetic pressure on the lagging current sheet. The results from the prototype thus show a high-density, high-temperature plasma of a rather large volume ($\approx$ a few cubic centimeters) can be confined for a long time (>5 μs) with the hypocycloidal-pinch apparatus. Energy confinement of tens of kilojoules and copious X-ray and neutron production in the HCP are expected when an adequate power source is used in the future.

The absorption of CO_2 laser energy can be used to determine the density of the plasma. For an underdense plasma, the dominant absorption process is that of inverse

bremsstrahlung due to electron-ion collisions. This process gives an absorption length (ref. 17):

$$l_{ab} = \frac{5 \times 10^{27} T_e^{3/2}}{n_e^2 Z \lambda^2} \left(1 - \frac{\lambda^2}{\lambda_e^2}\right)^{1/2}$$

Here λ is the wavelength in cm, λ_e is the wavelength in cm of radiation at the plasma electron frequency

$$\lambda_e = \frac{2\pi c}{\omega_e}$$

$$\omega_e^2 = \frac{4\pi n_e}{m_e}$$

T_e is the electron temperature in eV, n_e is the electron density in cm^{-3}, and Z is the ionic charge. By unfolding the relation $I = I_0 e^{-x/l_{ab}}$, n_e can be determined when T_e and Z are known. If $\lambda = \lambda_e$ or the plasma has a critical density, the absorption length is reduced to zero and near complete absorption will occur. In this case, if radiation of sufficient intensity falls on the plasma, it can create instabilities which lead to anomalous absorption of the radiation. For the plasma produced during the first compression in HCP, $T_e \approx 1$ keV and $Z = 1$ (since few impurity ion lines are observed above the continuum). Near complete absorption of the CO_2 laser ($\lambda = 10.6$ μm), that is, $I/I_0 < 0.01$, through a 5-cm-long plasma column indicates that the plasma column provided more than 4.6 times of the absorption length. This result can be translated into $n_e > 7.8 \times 10^{18}$ cm^{-3}. For the later times, the absorption of radiation takes place in the cold ($T_e < 100$ eV) and impurity-rich ($Z > 1$) plasma with its density $n_e < 10^{18}$ cm^{-3}. Because of the limit in the sensitivity of the IR detector system, the determination of the temporal variation of n_e was not possible.

The geometry of the HCP is such that there is easy access for laser or electron beam heating. Since the electron density of the plasma in the hypocycloidal pinch approaches the critical density for the CO_2 laser frequency, anomalous plasma heating to achieve thermonuclear fusion temperatures may be possible. This mechanism is predicted to be the most efficient for plasma heating. (See ref. 17.) Sufficiently powerful CO_2 lasers for this mechanism to be operational also have been developed. However, no other suitable plasma source has previously been available for testing the anomalous heating mechanism. (See ref. 17.) The dense plasma focus has been proposed as a plasma with sufficiently high density for testing the mechanism. (See ref. 18.) However, no successful experimental result has been reported to date. Its small volume and brief lifetime do not render clear observation of the effects of the interaction. The near complete absorption of CO_2 laser energy by the plasma in the HCP apparatus gives strong

encouragement of this approach although no apparent evidence for strong development of parametric instabilities, expected from the anomalous heating, is observed yet, perhaps because the energy (50 J) of the CO_2 laser used contributed only small fractions of the plasma energy of 900 J. It may be necessary to increase the laser output to the range of kilojoules to reach the "strong pump-field regime" for clear observation of the effect. (See ref. 19.)

Since the geometry of the hypocycloidal-pinch apparatus consists of a set of disks, a multiple array to form a linear or toroidal system could be constructed, as shown in figure 20. Such a system is not only capable of accommodating a large power, but will also improve the plasma containment time since the axial outflow will be reduced by the closed ends.

CONCLUSIONS

In conclusion, successful production of a long-lived high-density and high-temperature plasma in a large volume in the prototype of the hypocycloidal-pinch apparatus has been demonstrated. The plasma is observed to have near complete CO_2 laser energy absorption for a time larger than a quarter cycle of the discharge. The CO_2 laser absorption indicates plasma densities near 10^{19} in addition to the plasma temperature of 1 keV and the 5-μs plasma confinement time. It is optimistically suggested that this geometry could be adopted to develop a large-scale fusion-power reactor because of its advantages in plasma volume, containment time, easy access to additional heating by a laser or electron beams, and the possibility for scaling up to a multiple array.

Langley Research Center
National Aeronautics and Space Administration
Hampton, Va. 23665
December 2, 1975

APPENDIX A

SNOWPLOW MODEL FOR CURRENT SHELL IN A HYPOCYCLOIDAL PINCH

For this analysis only the upper chamber of the hypocycloidal-pinch apparatus is considered and it is treated as an independent circuit including the capacitor bank and the electrodes with a moving current sheet which is in the form of a cylindrical shell. Figure 21 shows the frame of coordinates (r,z) to be used. Also this analysis is limited to reveal the functional dependence of rundown speed on electrical and other parameters. Many assumptions are made to simplify the analysis.

In the MKS system of units and cylindrical coordinates (r,z), the equation of motion for a cylindrical current shell located at a radius r, as shown in figure 21, is

$$2\pi r \frac{B^2}{2\mu_o} h = \pi\rho h \frac{d}{dt}\left[\left(R^2 - r^2\right)\frac{dr}{dt}\right] \tag{A1}$$

where B is the magnetic induction induced by the current I; h, the height of the current shell; ρ, the density of the filling gas; and R, the radius of the chamber. This relationship is derived with the assumptions that the current shell is loaded with the mass $m = \pi\rho\left(R^2 - r^2\right)h$ "snowplowed" from the periphery of the chamber and that the thickness of the current shell is infinitely thin. Furthermore, the gas pressure ahead of the shell is assumed to be negligible compared with the magnetic pressure behind the current shell.

By Ampere's circuital law, $B = \mu_o I/(2\pi r)$ where $\mu_o = 4\pi \times 10^{-7}$ and equation (A1) becomes

$$\frac{d}{dt}\left[\left(R^2 - r^2\right)\frac{dr}{dt}\right] = -\frac{10^{-7}}{\pi\rho}\frac{I^2}{r} \tag{A2}$$

For the short time of interest, or a quarter cycle of the circuit oscillation, the sinusoidal current may be approximated with a linearly rising current $I = (dI/dt)_{av}t$ where $(dI/dt)_{av}$ is the rate of current rise. The dimensionless variables are introduced:

$$x = \frac{r}{R}$$

$$T = \frac{t}{T_k}$$

where

$$T_k^4 = \frac{\pi\rho R^4}{10^{-7}\left(\frac{dI}{dt}\right)_{av}^2} \tag{A3}$$

Then equation (A2) can be reduced to

$$\frac{d}{dT}\left[\left(1 - x^2\right)\frac{dx}{dT}\right] = -\frac{T^2}{x} \tag{A4}$$

The $x(T)$ determines the shape of radius-time curves for the radially advancing current shell. The numerical integration of equation (A4) may be found elsewhere. (See ref. 20.)

The speed of the current sheet $V_r = dr/dt$ is related by

$$\frac{dr}{dt} = \frac{R}{T_k}\frac{dx}{dT} \tag{A5}$$

The constant R/T_k is

$$\frac{R}{T_k} = \left[\frac{10^{-7}\left(\frac{dI}{dt}\right)_{av}^2}{\pi\rho}\right]^{1/4} \tag{A6}$$

Therefore, the initial conditions of the system have the following functional relations with the speed V_r of the current shell:

(1) The radial speed of the current shell varies with the gas density as

$$V_r \propto \rho^{-1/4} \tag{A7}$$

Since ρ is proportional to the pressure of the gas p,

$$V_r \propto p^{-1/4}$$

(2) The radial speed V_r is proportional to square root of the rate of current rise

$$V_r \propto \left(\frac{dI}{dt}\right)_{av}^{1/2} \tag{A8}$$

For a pure oscillatory circuit, or L-C circuit, the peak current I_p is

$$I_p = EC^{1/2}L^{-1/2} \tag{A9}$$

where E is the charging voltage. The quarter period $T_{1/4}$ is

$$T_{1/4} = \frac{\pi}{2} L^{1/2} C^{1/2} \tag{A10}$$

The average rate of current rise is

$$\left(\frac{dI}{dt}\right)_{av} = \frac{I_p}{T_{1/4}} = \frac{2}{\pi} \frac{E}{L} \tag{A11}$$

Therefore,

$$V_r \propto \left(\frac{E}{L}\right)^{1/2} \tag{A12}$$

This relationship indicates that it is desirable to have a high-voltage and low-inductance circuit to obtain a high current-sheet velocity.

APPENDIX B

INFRARED DETECTOR SENSITIVITY

When the IR detector is located at a distance r from the plasma, which is irradiated by a laser with a power I_o, the intensity I_{sd} of the scattered laser power entering the detector is

$$I_{sd} = \left(\frac{I_s}{4\pi r^2}\right)A \tag{B1}$$

where A is the area of the entrance window of the detector, and I_s is the total scattered laser power, or $I_s = \eta I_o$ where η is total scattering cross section. Here it is assumed that the scattering is isotropic.

The current i in the detector resulting from I_{sd} is

$$i = SI_{sd} \tag{B2}$$

where S is the current responsivity of the detector or

$$i = S\eta I_o \frac{A}{4\pi r^2} \tag{B3}$$

The resulting voltage E across a load impedance Z is

$$E = Zi$$

or

$$E = ZS\eta \frac{I_o A}{4\pi r^2} \tag{B4}$$

The IR 2 detector used in the experiment has the parameters:

$$Z = \frac{R}{\left(1 + \frac{f^2}{f_c{}^2}\right)^{1/2}} = 1.7 \times 10^4\ \Omega$$

where the load resistance is

$$R = 10^6\ \Omega$$

the laser modulation frequency is

$$f = 2.5 \times 10^6/s$$

and the detector response frequency is

$$f_c = \frac{1}{2\pi Rc} = 3.18 \times 10^4/s$$

and

$$S = 0.1 \times 10^{-6}\ A/W$$

$$I_o = 5 \times 10^8\ W \text{ or } 50\ J \qquad \text{(delivered by 100-ns pulse)}$$

$$A = 10^{-4}\ \pi\ m^2 \qquad \text{(2-cm-diameter window)}$$

$$r = 1\ m$$

The scattering cross section η can be determined from the equation by

$$\eta = \frac{4\pi r^2 E}{RSI_oA} = 5 \times 10^{-1}\ E \tag{B5}$$

by using the measured voltage E. Since the responsive voltage of 0.01 V above the noise level on the detector signal is clearly observable on a cathode ray oscilloscope, a scattering cross section as small as 5×10^{-3} can be determined. However, for the IR 2 located in the 90^o direction, the plasma is viewed through a hole with a 3-mm diameter and a reduction of the scattered power by a factor of $\approx$20 is estimated. To overcome this reduction in the system sensitivity, a 10-cm-diameter germanium lens is inserted on the optical path to collect the scattered laser power. The use of the lens results in a gain of 25. Therefore, the minimum scattering cross section detectable in the 90^o direction is

$$\eta_{min}(90^o) = 4 \times 10^{-3}$$

When the detector is located in the 10^o direction, the entire plasma is viewed and the minimum cross section detectable without a collection lens is

$$\eta_{min}(10^o) = 5 \times 10^{-3}$$

REFERENCES

1. Filippov, N. V.; Filippova, T. I.; and Vinogradov, V. P.: Dense, High-Temperature Plasma in a Noncylindrical z-Pinch Compression. CN-10/226, Nuclear Fusion: 1962 Supplement, Pt. 2, 1962, pp. 577-583.

2. Bottoms, P. J.; Carpenter, J. P.; Mather, J. W.; Ware, K. D.; and Williams, A. H.: On the Mechanism of Neutron Production From the Dense Plasma Focus. CN-24/G-5, Third Conference on Plasma Physics and Controlled Nuclear Fusion Research (Novosibirsk, USSR), Aug. 1968.

3. Lee, J. H.; Shomo, L. P.; Williams, M. D.; and Hermansdorfer, H.: Neutron Production Mechanism in a Plasma Focus. Phys. Fluids, vol. 14, no. 10, Oct. 1971, pp. 2217-2223.

4. Maisonnier, Ch.; Pecorella, F.; Rager, J. P.; Samuelli, M.; Strangio, C.; and Messina, A.: Comparative Studies of Plasma Focus Devices. IAEA-33/E6-2, Fifth Conference on Plasma Physics and Controlled Nuclear Fusion Research (Tokyo, Japan), Nov. 1975.

5. Conrads, H.; Cloth, P.; Demmeler, M.; and Hecker, R.: Velocity Distribution of the Ions Producing Neutrons in a Plasma Focus. Phys. Fluids, vol. 15, no. 1, Jan. 1972, pp. 209-211.

6. Imshennik, V. S.; Filippov, N. V.; and Filippova, T. I.: Similarity Theory and Increased Neutron Yield in a Plasma Focus. Nuclear Fusion, vol. 13, no. 6, Dec. 1973, pp. 929-934.

7. Mather, J. W.: Formation of a High-Density Deuterium Plasma Focus. Phys. Fluids, vol. 8, no. 2, Feb. 1965, pp. 366-377.

8. Andrianov, A. M.; Bazilevskaia, O. A.; Braginskii, S. I.; Brezhnev, B. G.; Khavaschevski, S.; Khrabrov, V. A.; Kovalski, N. G.; Filippov, N. V.; Filippova, T. I.; Palchikov. V. E.; Podgorny, I. M.; Prokhorov, Yu. G.; and Sulkovskaya, M. M.: High-Current Pulse Discharges. Second U.N. International Conference on the Peaceful Uses of Atomic Energy, vol. 31, U.N. (Geneva, Switzerland), 1958, pp. 348-364.

9. Lee, J. H.; and McFarland, D. R.: Hypocycloidal Focus. Bull. Amer. Phys. Soc., vol. 18, no. 10, Ser. II, Oct. 1973, p. 1369.

10. Lee, J. H.; and McFarland, D. R.: Diagnostic Measurements on a Hypocycloidal Pinch. Bull. Amer. Phys. Soc., vol. 19, no. 9, Ser. II, Oct. 1974, p. 946.

11. Mayer, F. J.: The Spindle Focus – Preliminary Considerations of Locational Sta-Stability. Bull. Amer. Phys. Soc., vol. 15, no. 11, Ser. II, Nov. 1, 1970, p. 1462.

12. Ware, K. D.; and Mather, J. W.: Radial Collapse of a Dense Plasma Spindle Focus. LA-5178-MS, U.S. Atomic Energy Com., Apr. 1973.

13. Rosenbluth, M.: Infinite Conductivity Theory of the Pinch. LA-1850, U.S. Atomic Energy Com., Sept. 1954.

14. Elton, R. C.; and Anderson, A. D.: Calculations Useful in the Determination of Electron Temperature From X-Ray Continuum Radiation Emitted From High Temperature Plasmas. NRL Rep. 6541, U.S. Navy, Mar. 31, 1967.

15. Elton, R. C.: Determination of Electron Temperatures Between 50 eV and 100 keV From X-Ray Continuum Radiation in Plasmas. NRL Rep. 6738, U.S. Navy, Dec. 11, 1968.

16. Griem, Hans R.: Plasma Spectroscopy. McGraw-Hill Book Co., Inc., 1964.

17. Dawson, J. M.; Hertzberg, A.; Kidder, R. E.; Vlasses, G. C.; Ahlstrom, H. G.; and Steinhauer, L. C.: Long-Wavelength, High-Powered Lasers for Controlled Thermonuclear Fusion. IAEA-CN-28/D-13, Fourth Conference on Plasma Physics and Controlled Nuclear Fusion Research (Madison, Wisconsin), June 1971, pp. 673-687.

18. Shatas, Romas A.; Stettler, John D.; Meyer, Harry C.; and Roberts, Thomas G.: Soft X Rays From a Laser-Heated Dense Plasma Focus. J. Appl. Phys., vol. 42, no. 13, Dec. 1971, pp. 4885-5886.

19. Kruer, W. L.; and Dawson, J. M.: Anomalous High-Frequency Resistivity of a Plasma. Phys. Fluids, vol. 15, no. 3, Mar. 1972, pp. 446-453.

20. Artsimovich, L. A.: Controlled Thermonuclear Reactions. Gordon & Breach, Sci. Publ., Inc., 1964.

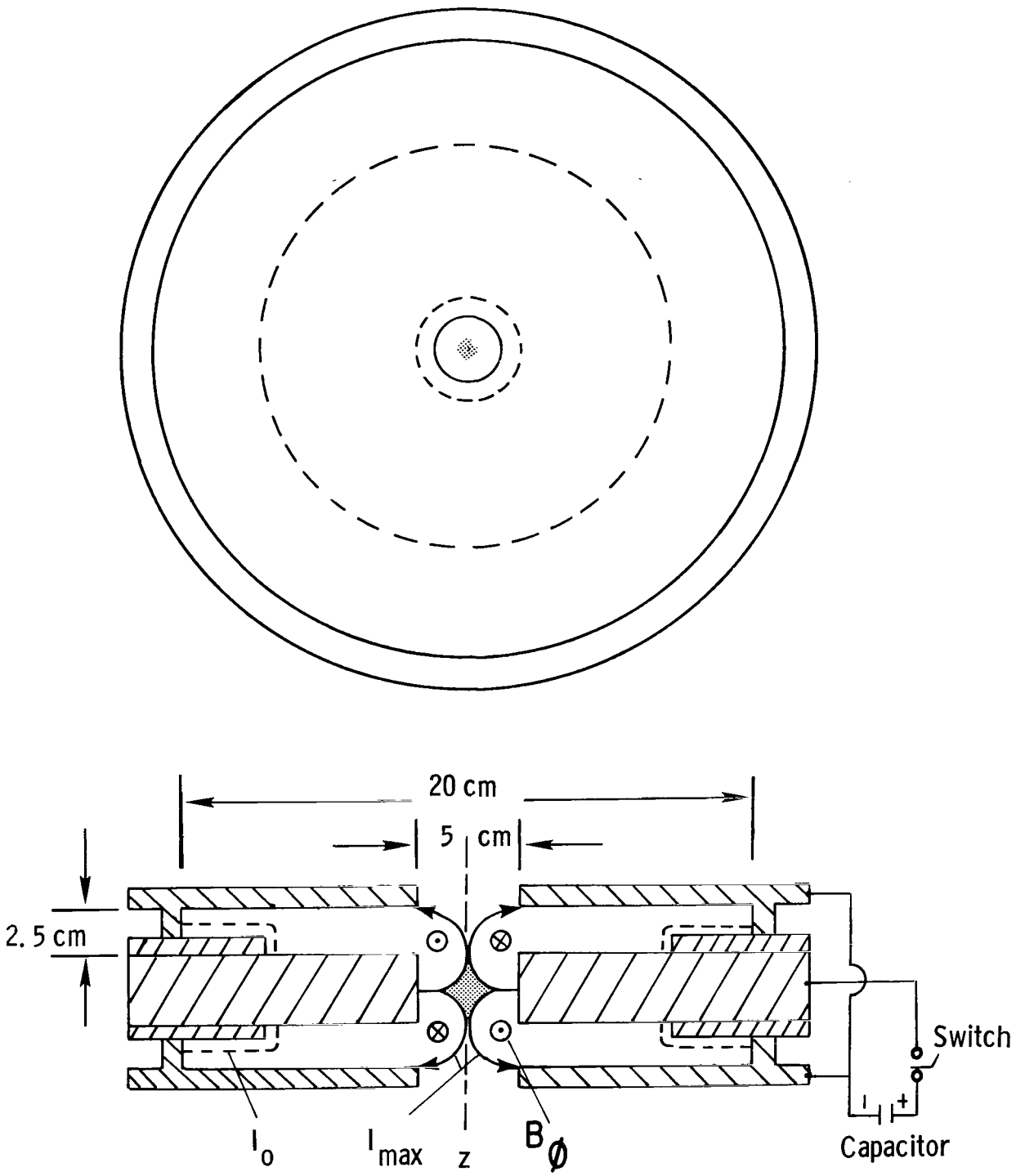

Figure 1.- Plan view of the cross section of hypocycloidal-pinch apparatus.

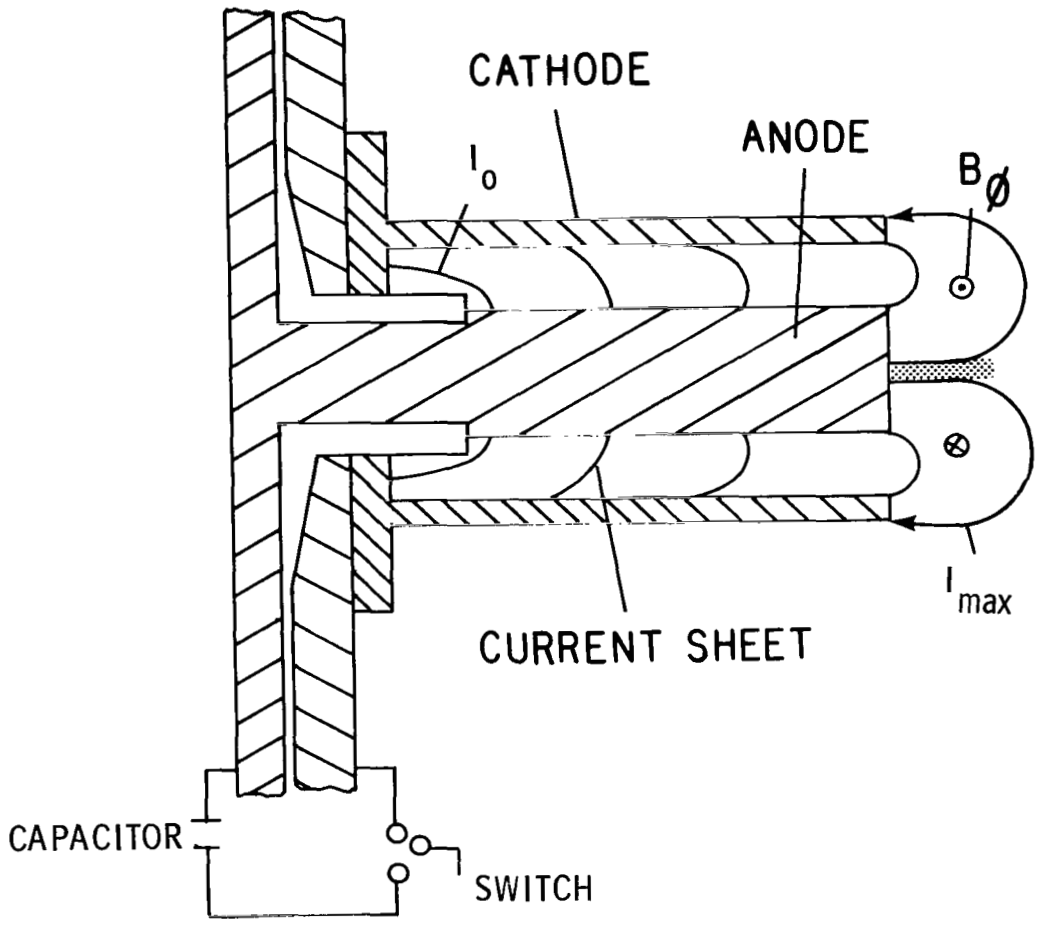

Figure 2.- A dense plasma focus apparatus.

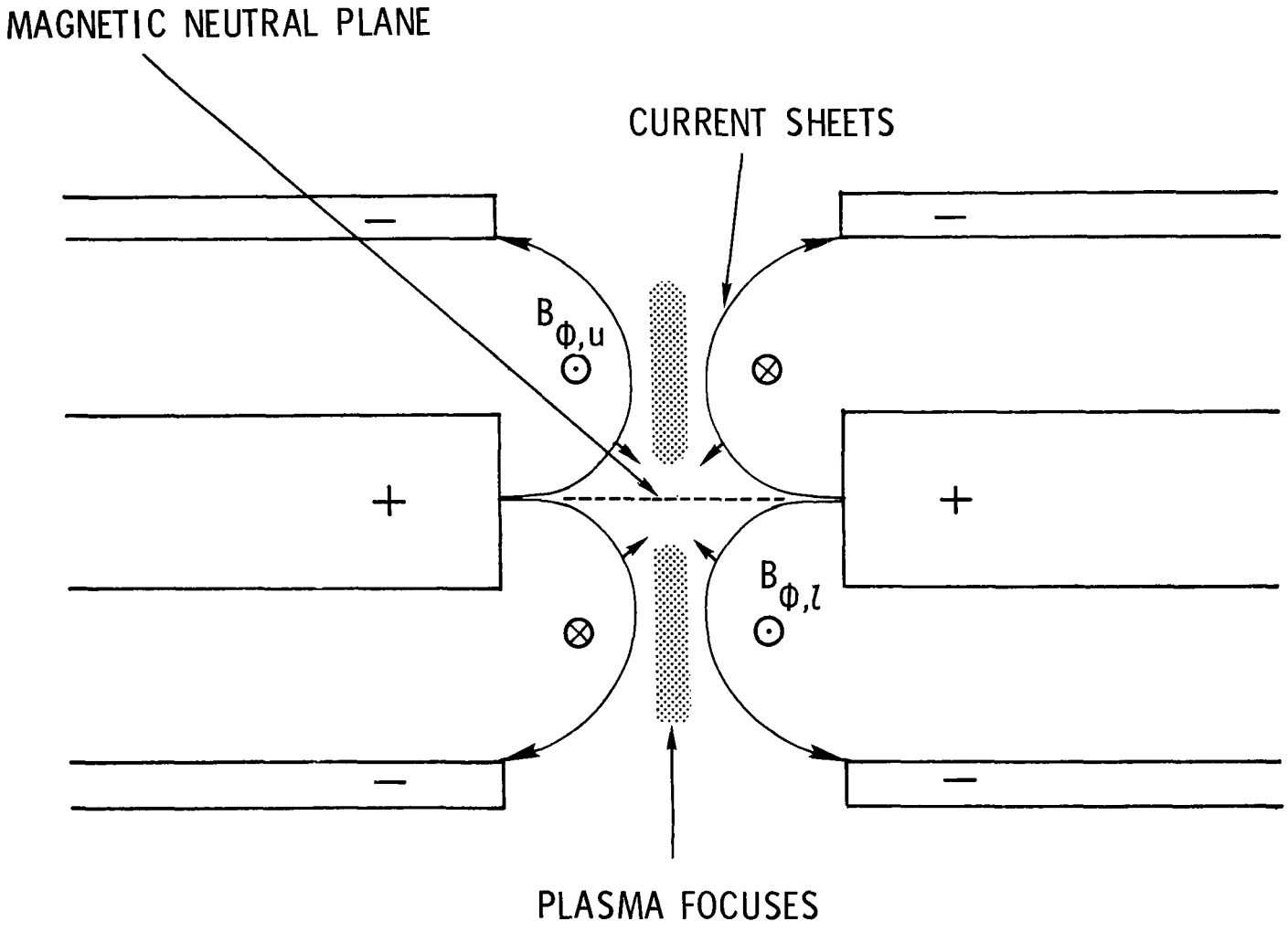

Figure 3.- Current and magnetic configuration in the center. $B_{\phi,u}$ and $B_{\phi,l}$ are the azimuthal magnetic induction of the upper and the lower chambers, respectively.

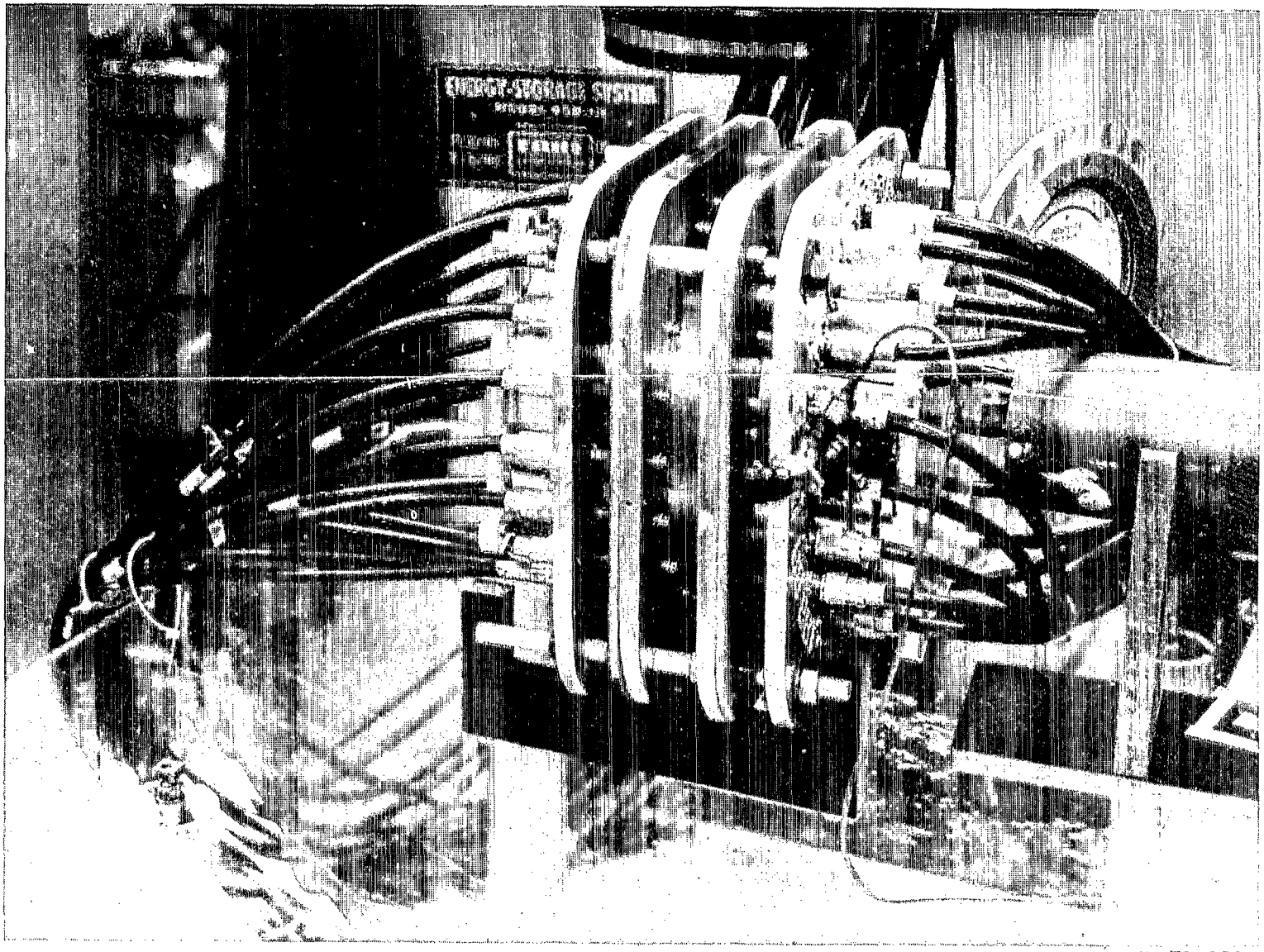

L-73-6690

Figure 4.- The 20-cm-diameter prototype.

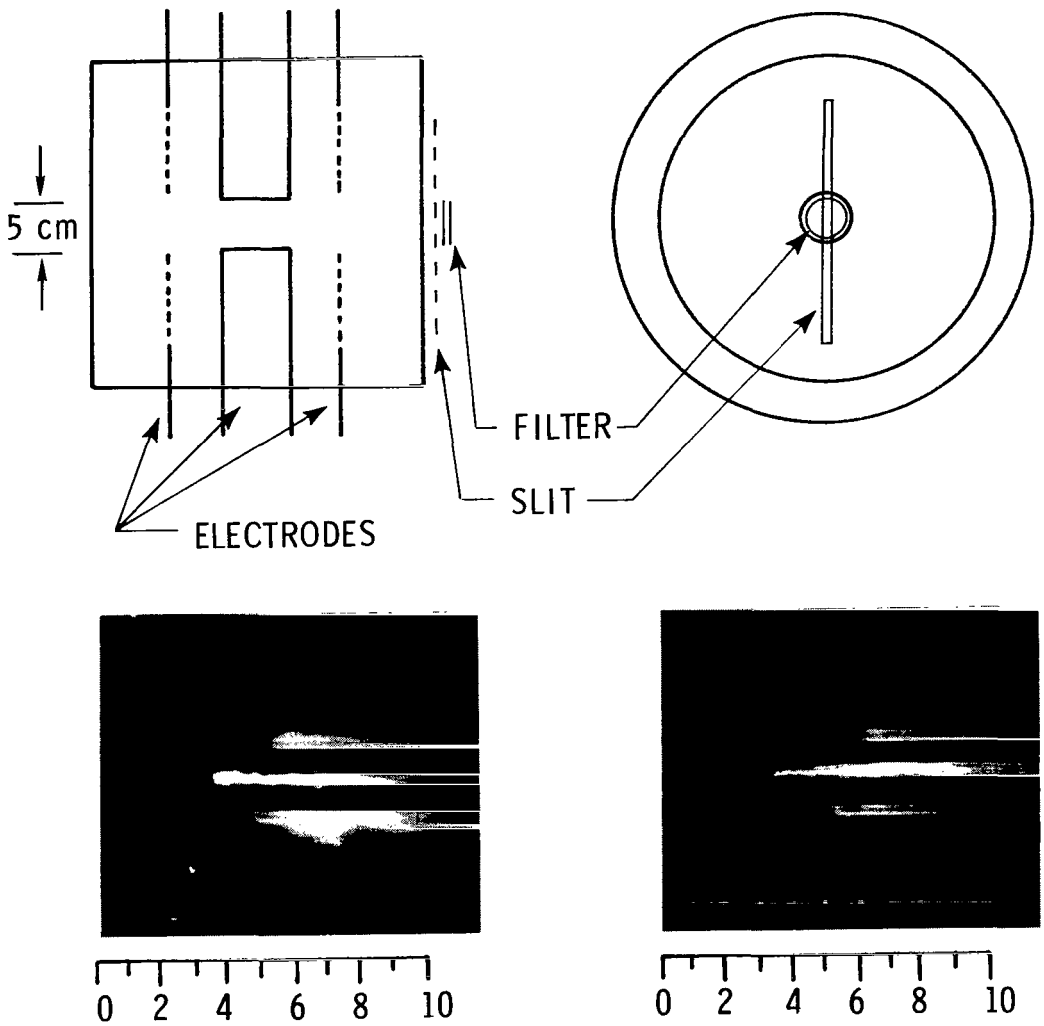

L-75-253

Figure 5.- Streak pictures of plasma produced in HCP. Reproducibility is shown by pictures of two different runs.

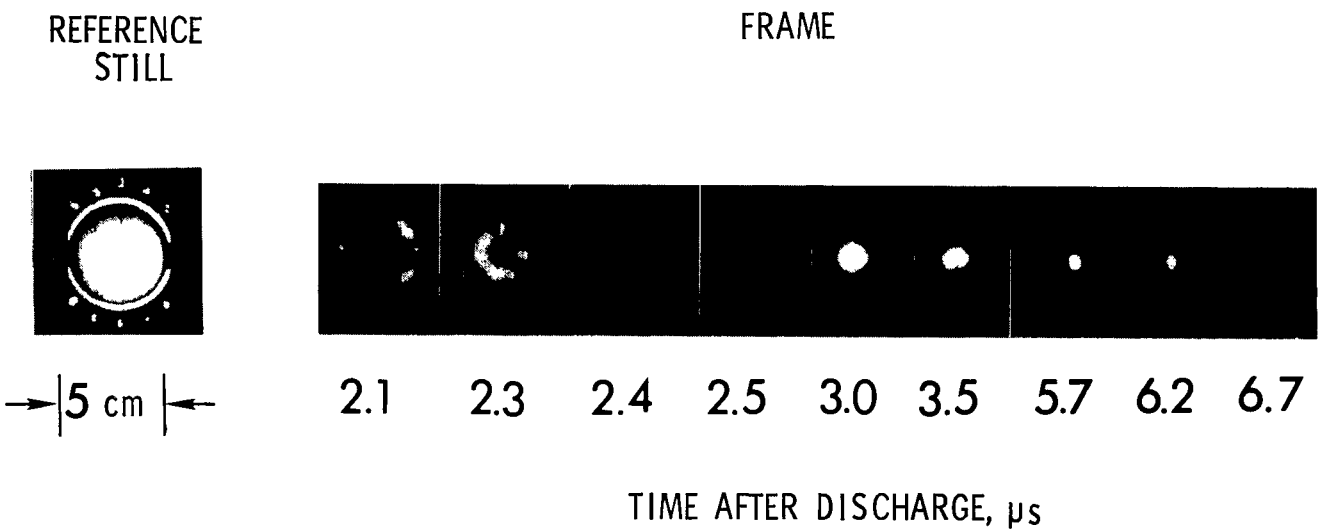

L-75-254

Figure 6.- Frame pictures of the current-sheet compression and dense plasma production. Different neutral density filters with increasing density were used to obtain proper exposure.

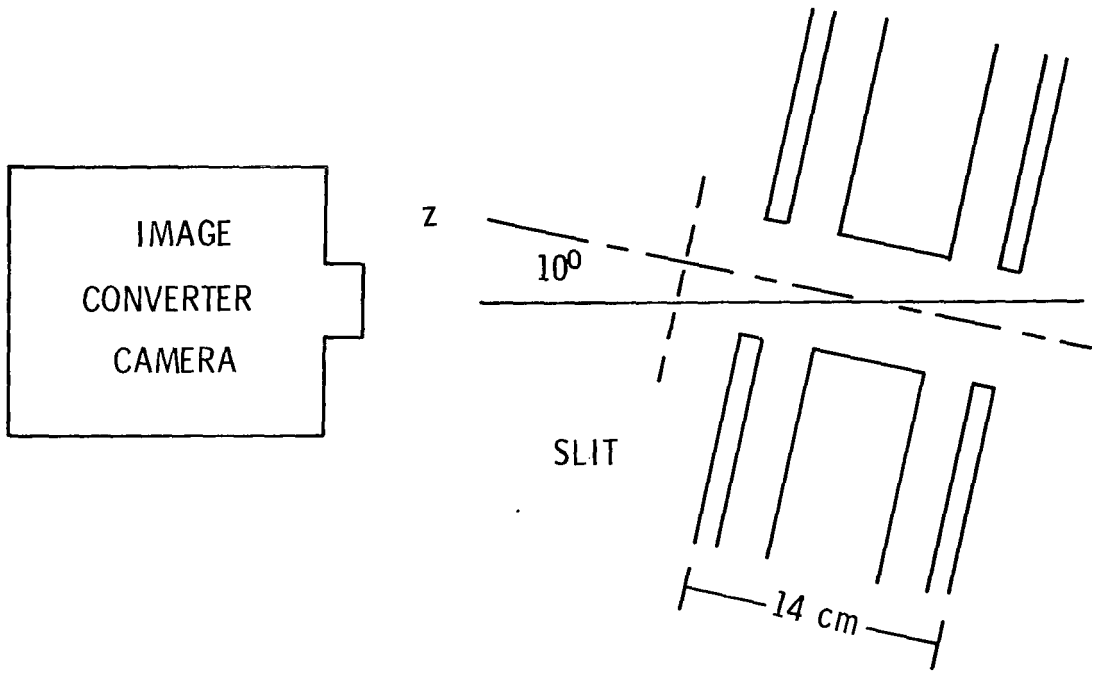

(a) Optical setup.

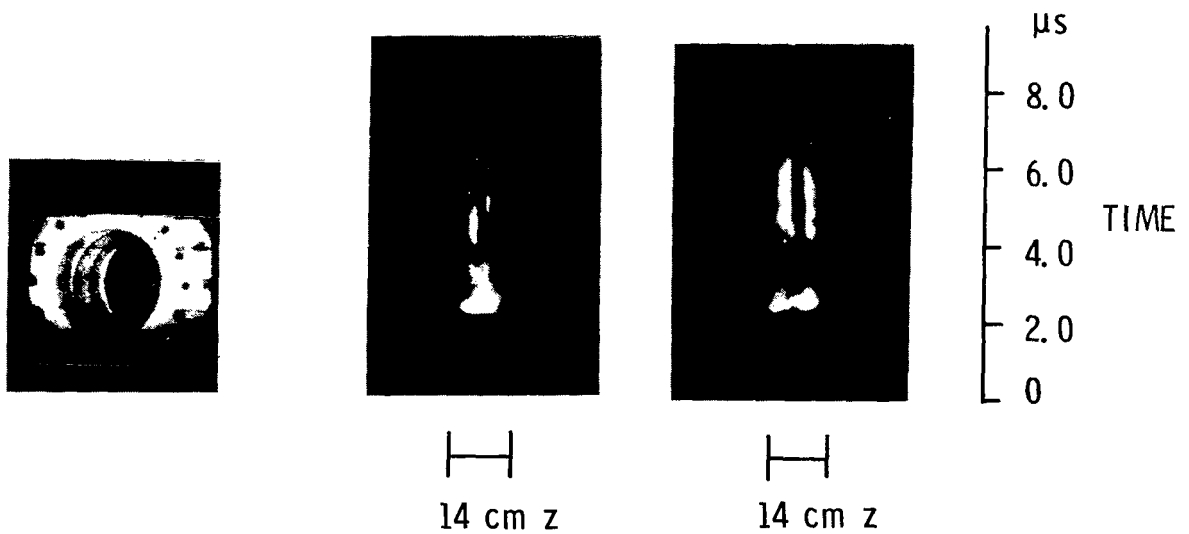

(b) Still reference. (c) Streak. (d) Streak.

L-75-255

Figure 7.- Axial motion of plasma focuses in center hole is observed with camera aimed 10° off axis.

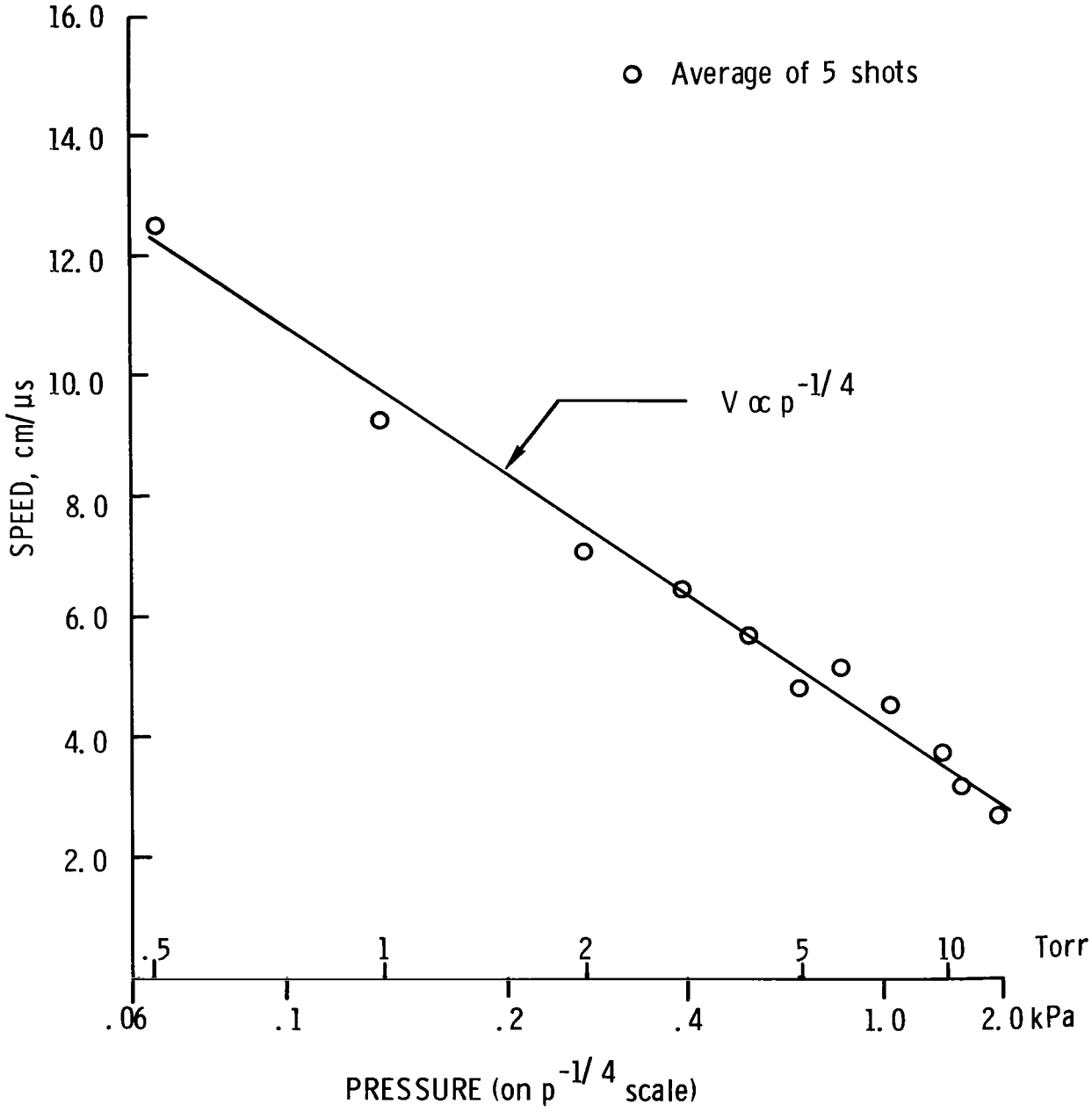

Figure 8.- Rundown speed of current sheets as function of filling pressure.

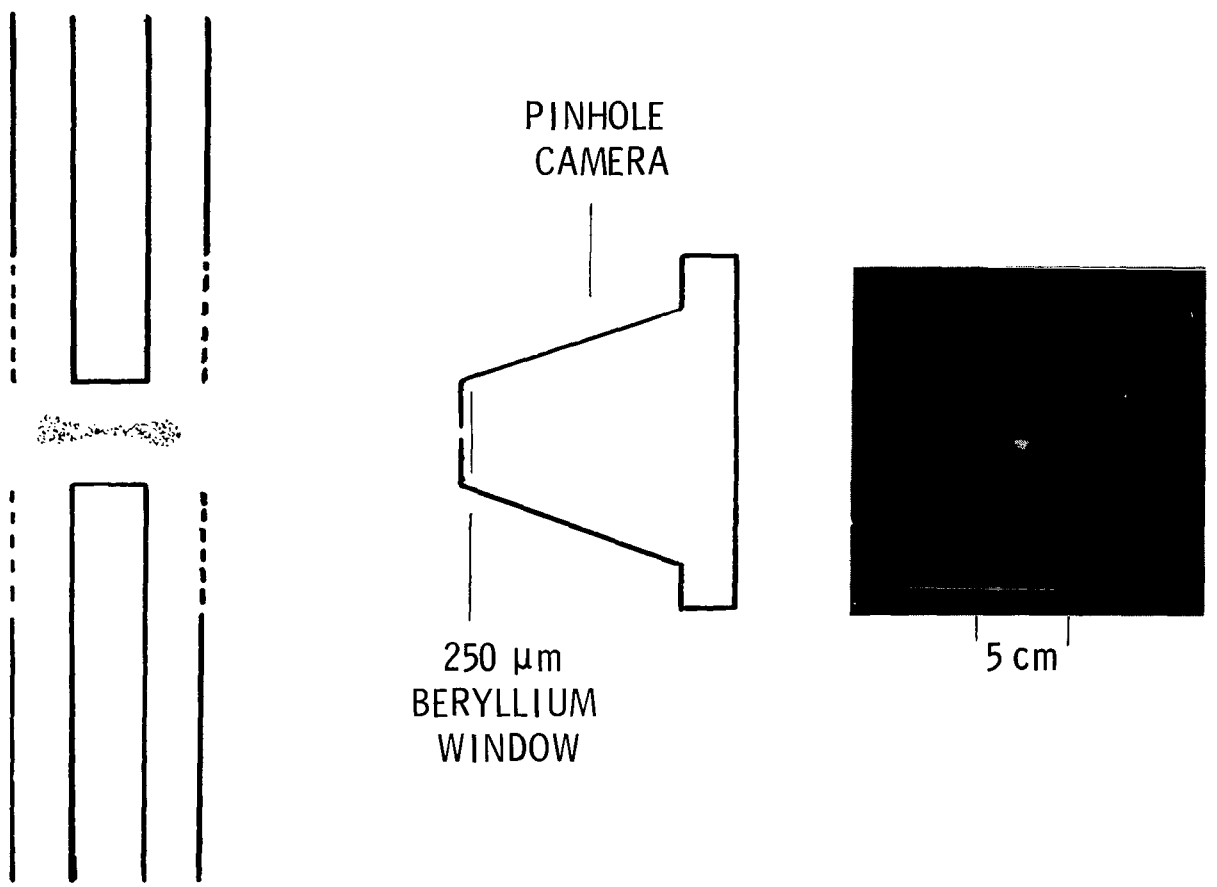

L-75-256

Figure 9.- X-ray pinhole photograph of plasma.

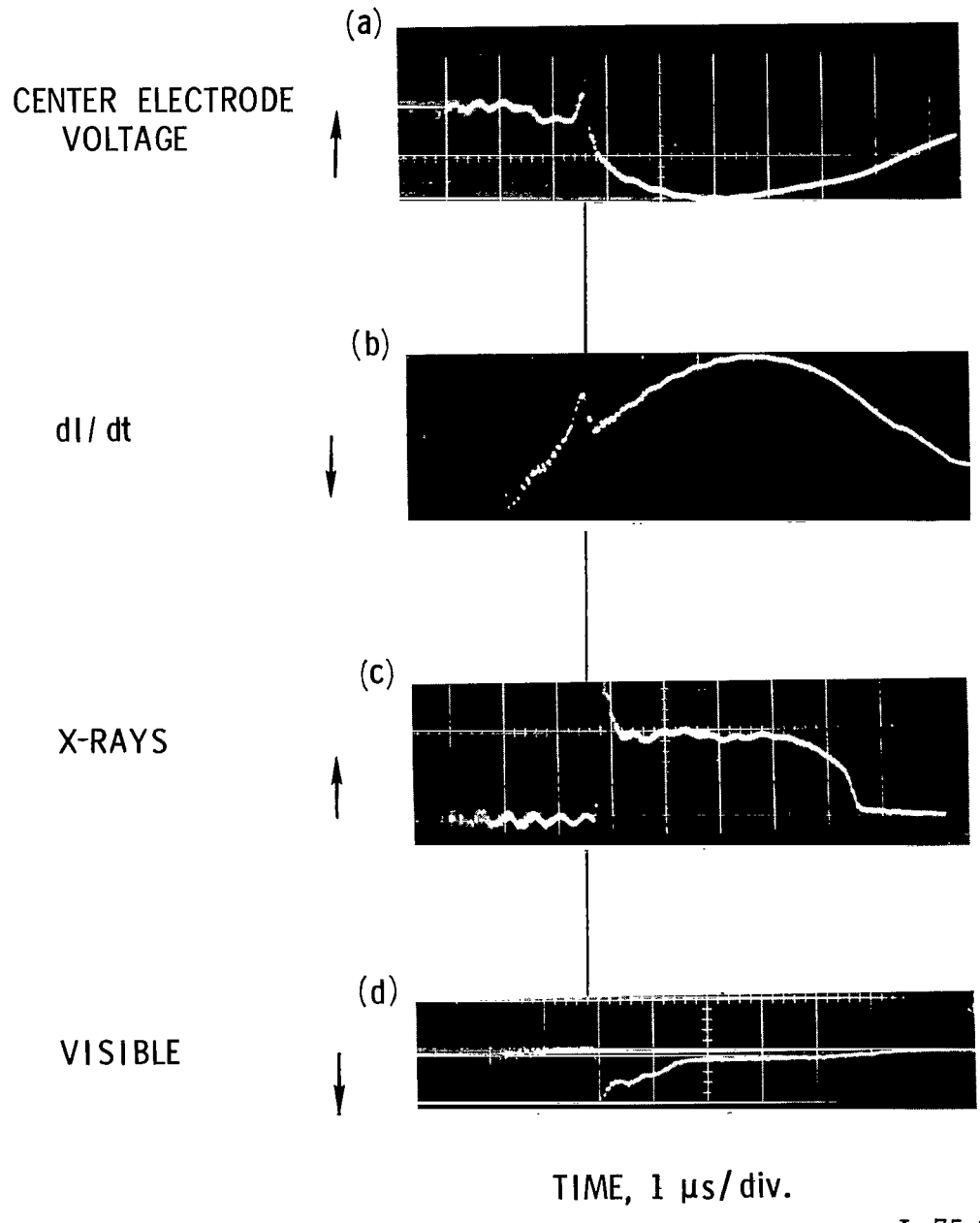

L-75-257

Figure 10.- Temporal evolution of the various events of hypocycloidal pinch.

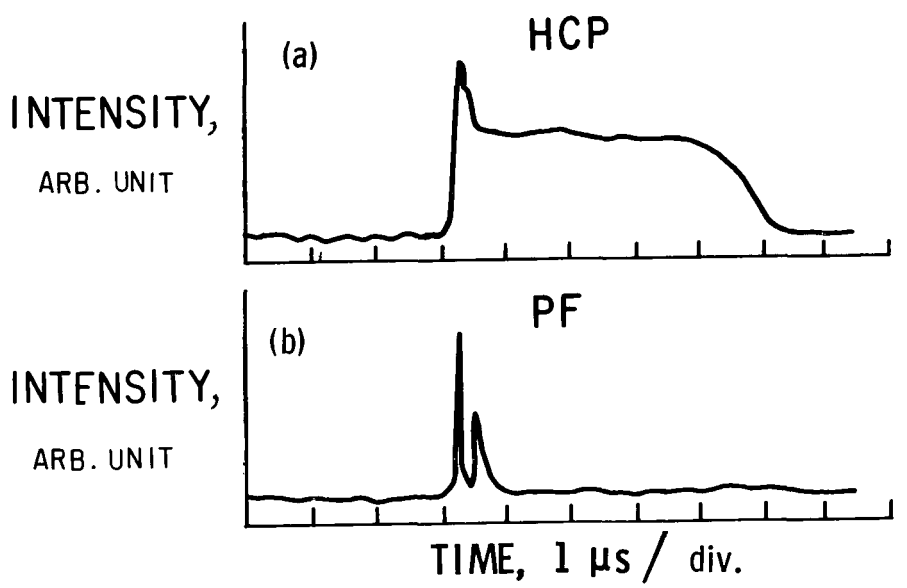

Figure 11.- Comparison of X-ray emission of hypocycloidal pinch and dense plasma focus.

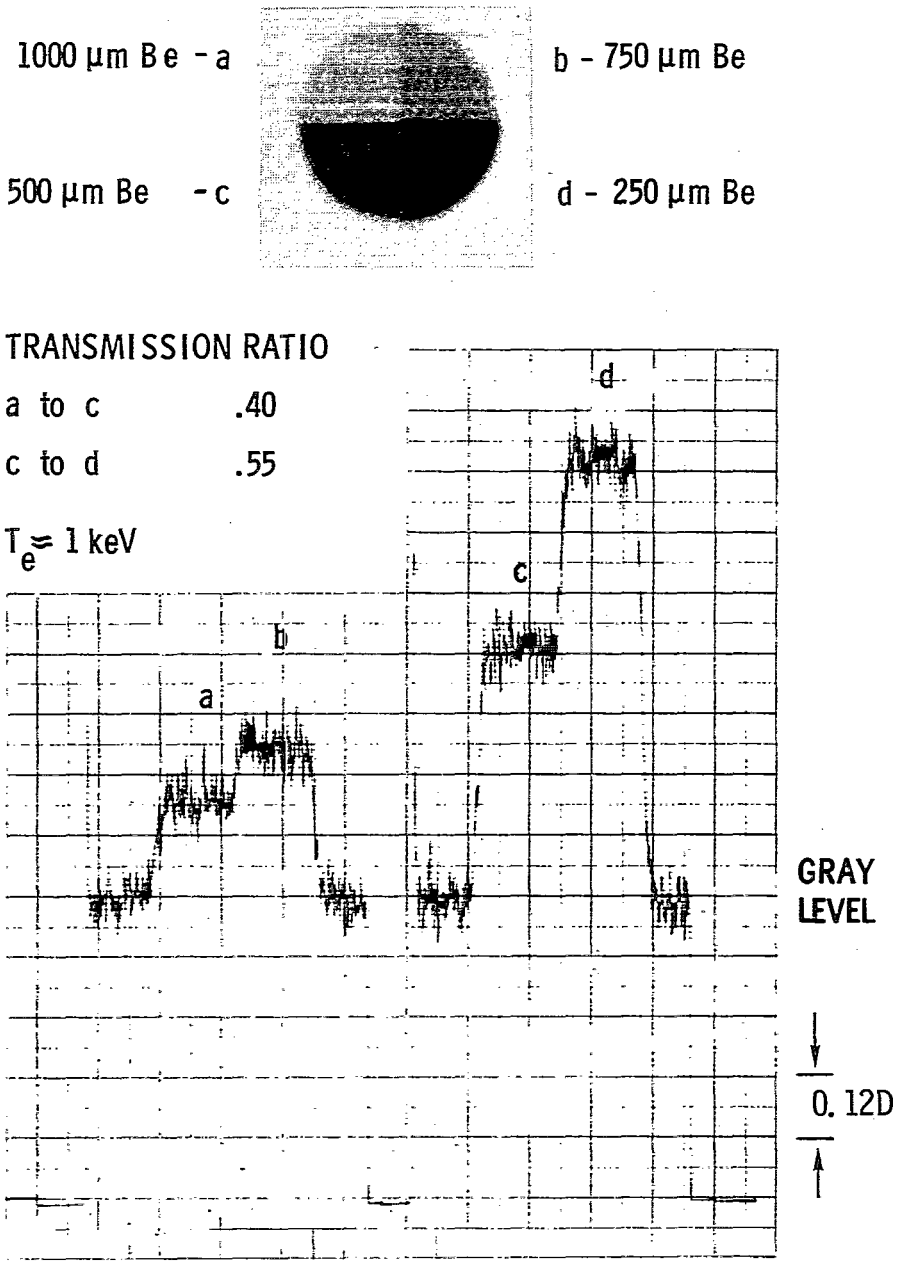

Figure 12.- Densitometer trace of exposed film showing differential X-ray transmission through various thicknesses of Be foil. The electron temperature is estimated from transmission ratio.

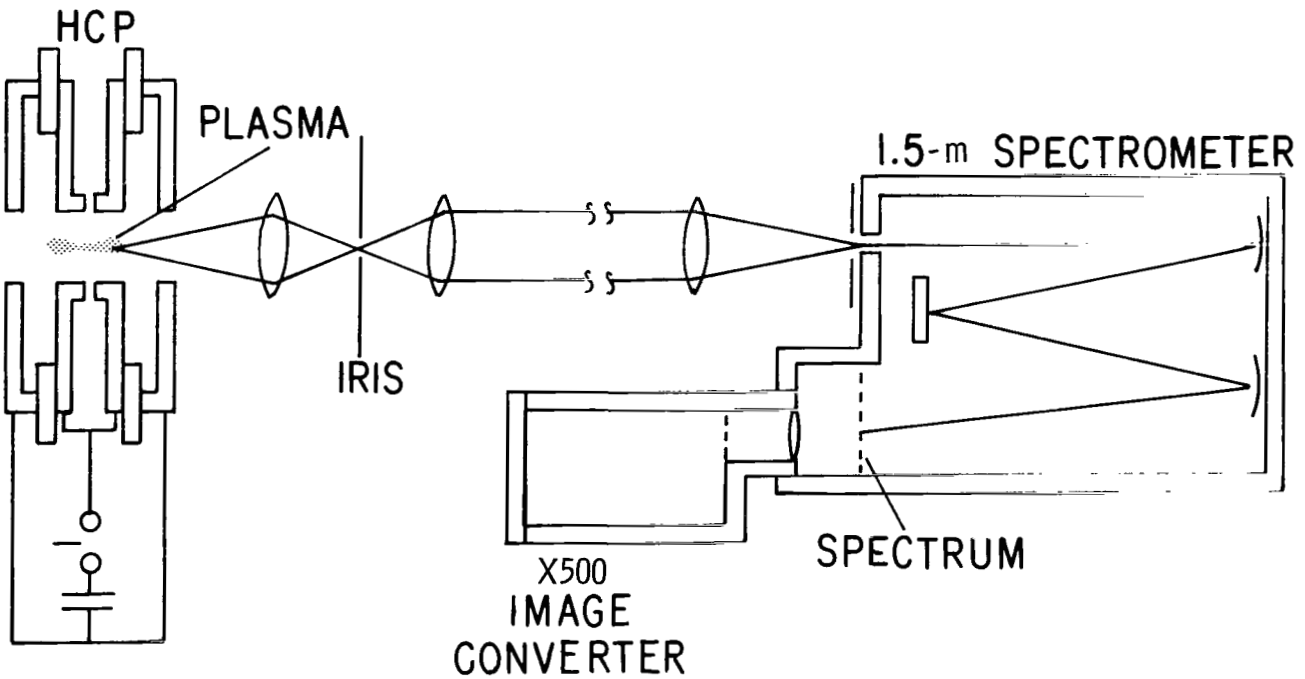

Figure 13.- Image-converter camera-spectrometer system used to observe time-resolved spectra.

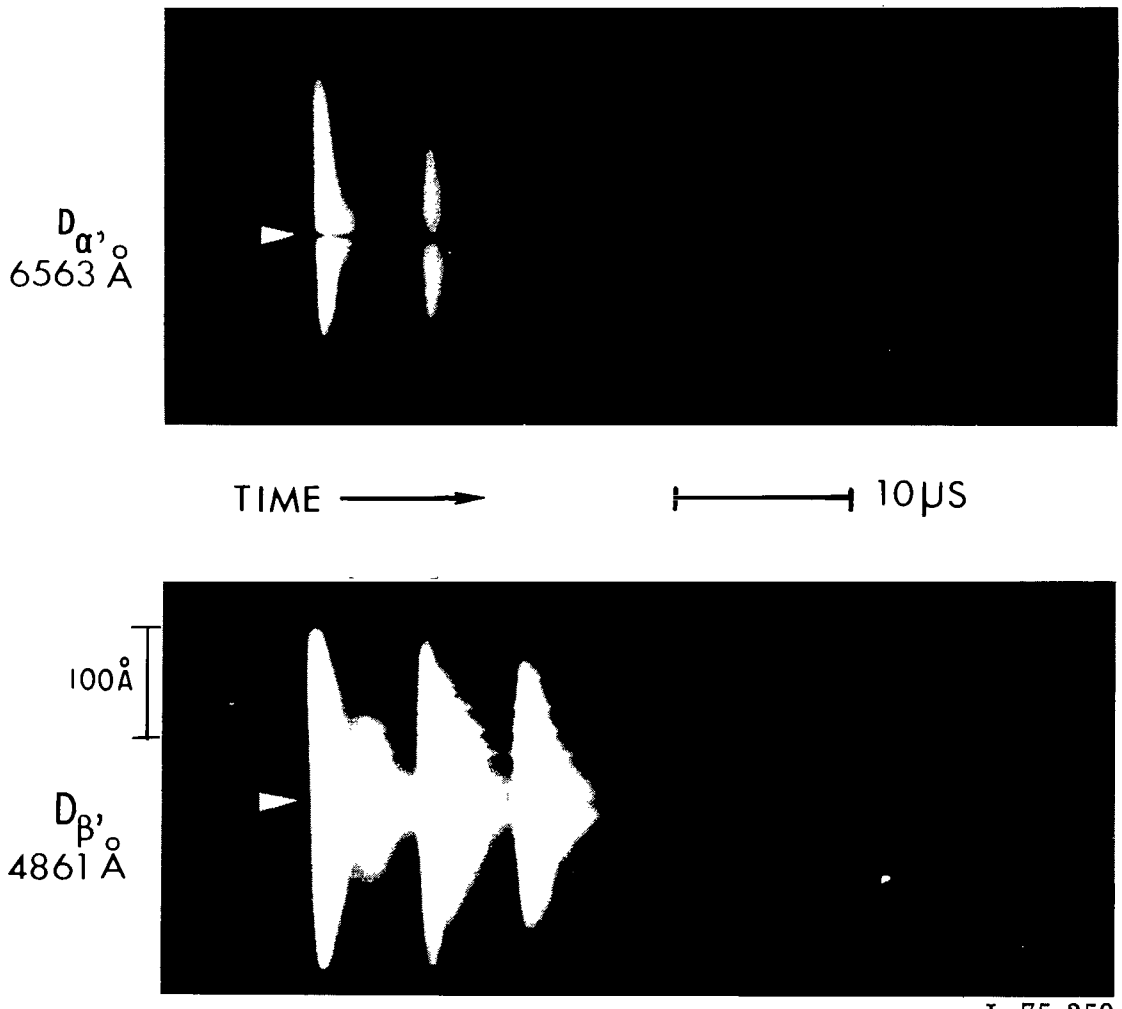

Figure 14.- Line broadening seen in time-resolved spectrum.

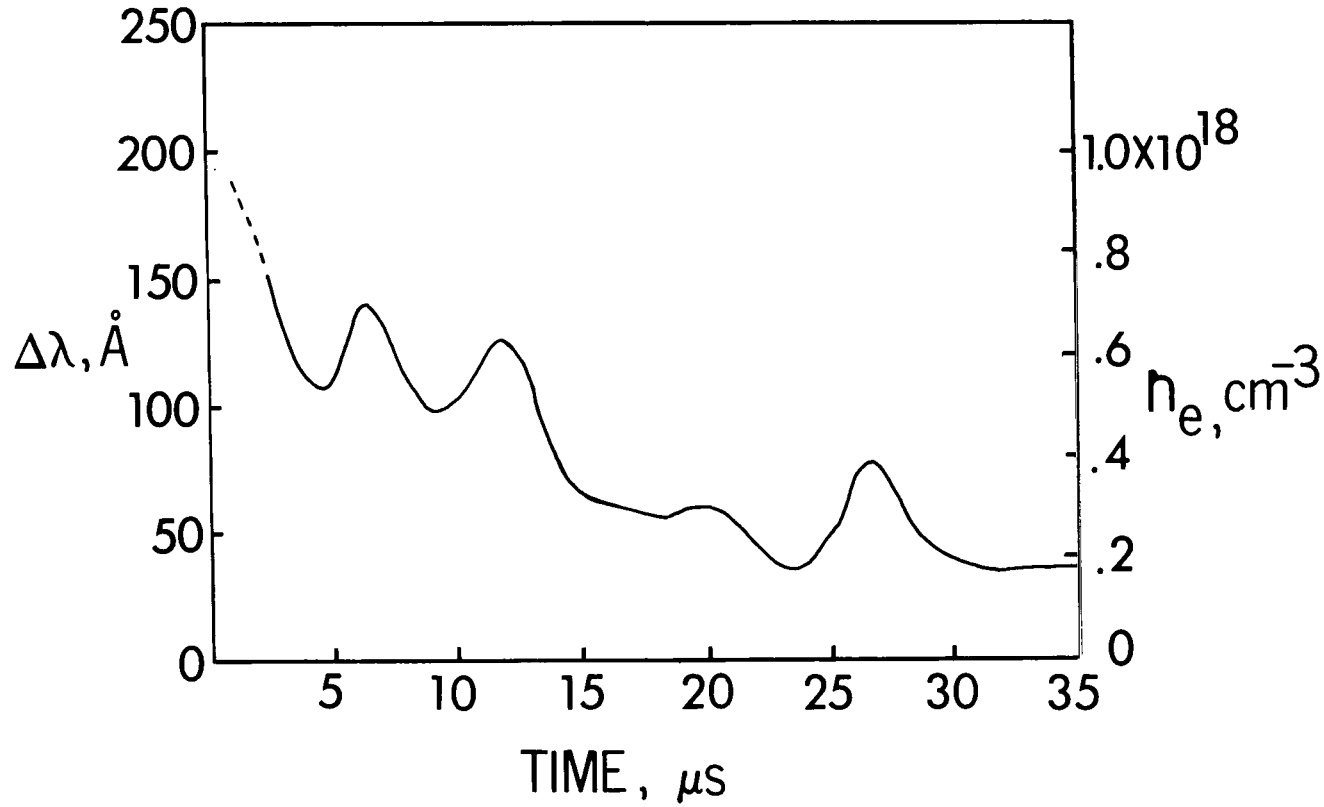

Figure 15.- Plasma density variation in time measured with half-width $\Delta\lambda$ of D_α line broadening.

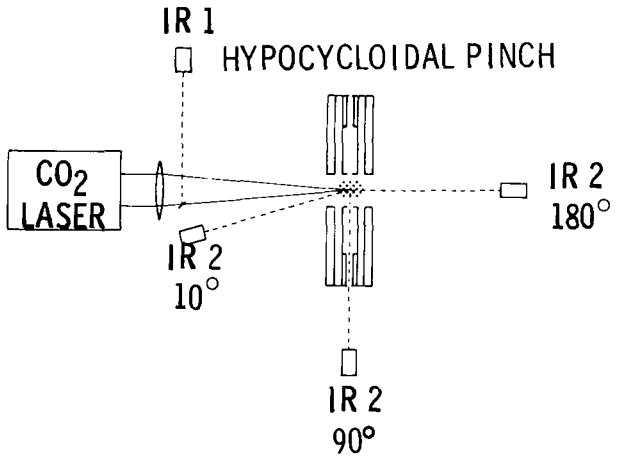

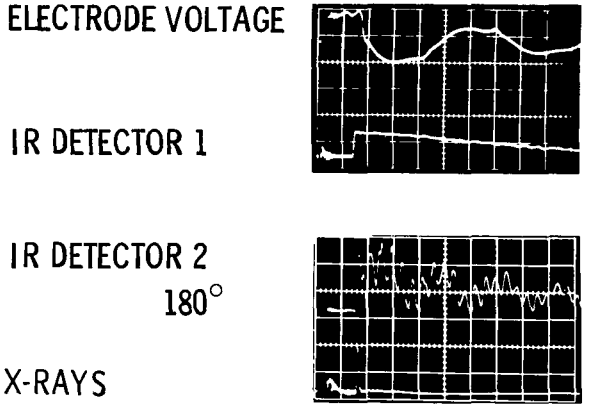

(a) t = -0.2μs.

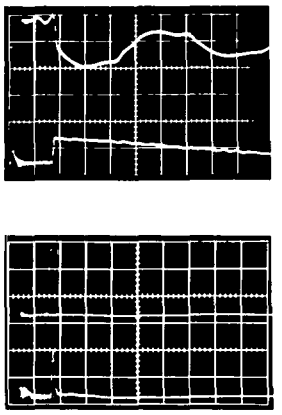

TIME, 2 μs/div.

(b) t = 0.

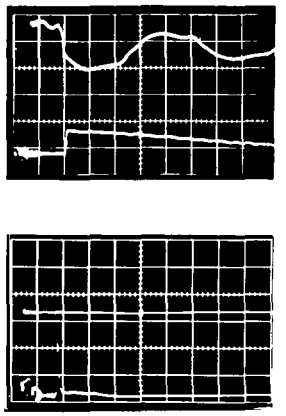

TIME, 2 μs/div.

(c) t = 0.5 μs.

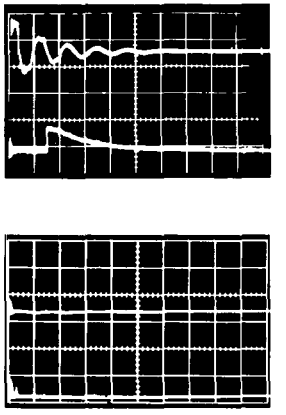

TIME, 10 μs/div.

(d) t = 12 μs.

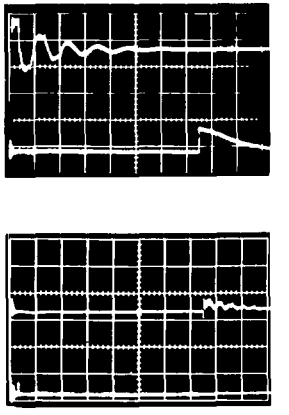

TIME, 10 μs/div.

(e) t = 72 μs.

L-75-260

Figure 16.- Experimental setup and results of CO_2 laser absorption experiment.

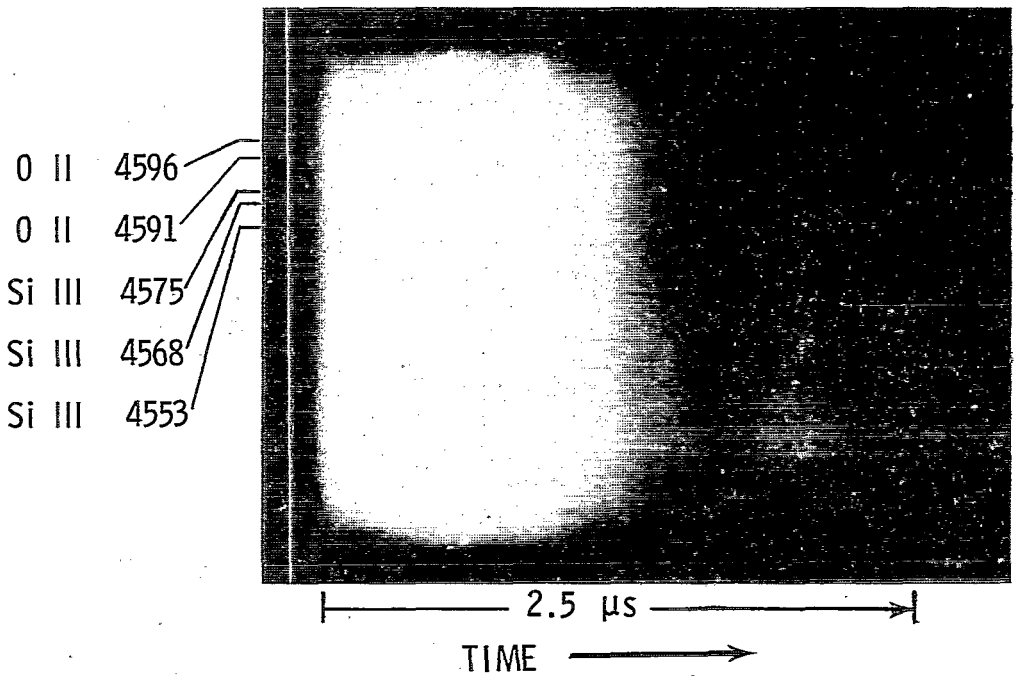

L-75-261

Figure 17.- Time-resolved spectrum observed in first collapse. No line radiation is apparent during first 1 μs. O and Si lines appear later in time.

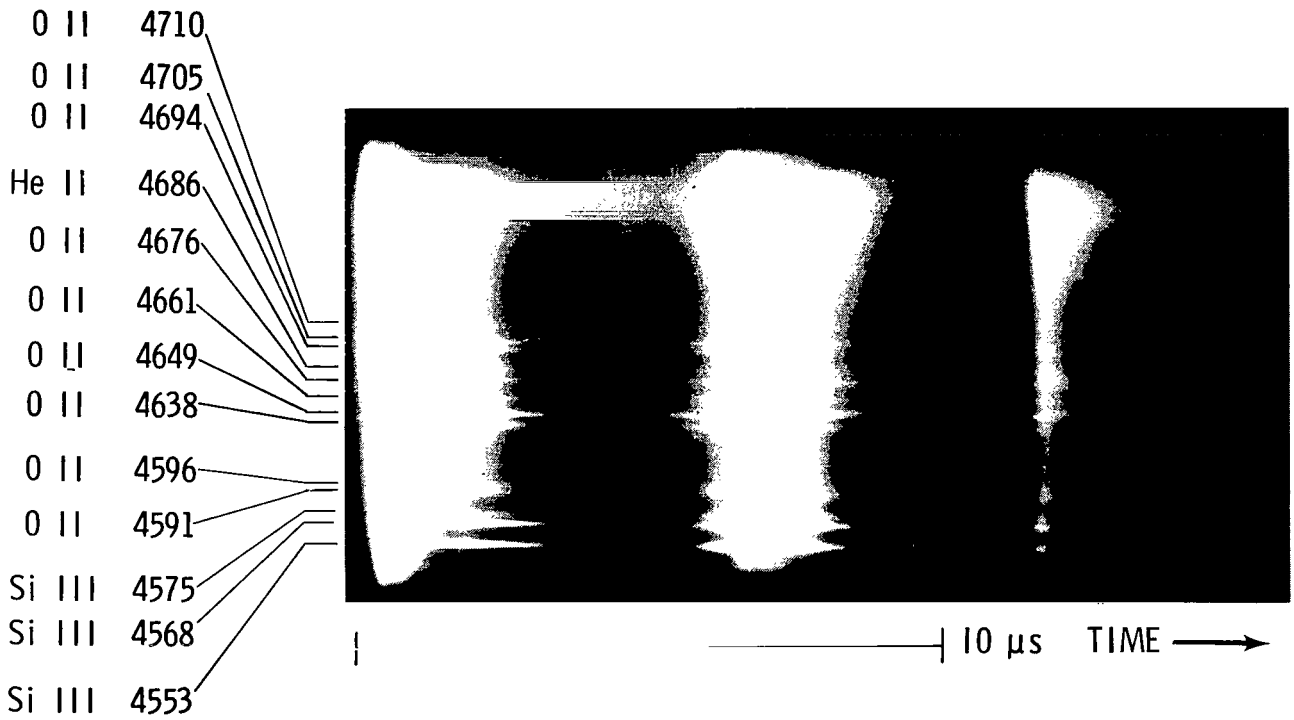

L-75-262

Figure 18.- Identified impurity lines.

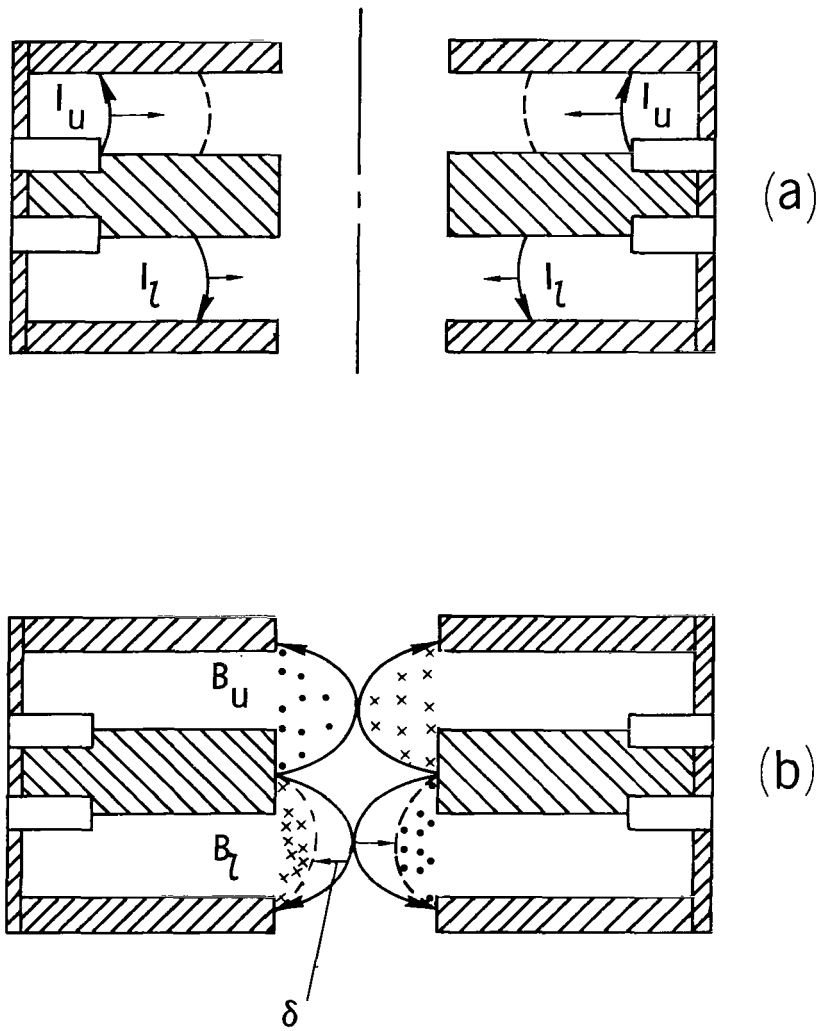

Figure 19.- Self-stabilizing mechanism of hypocycloidal-pinch configuration.

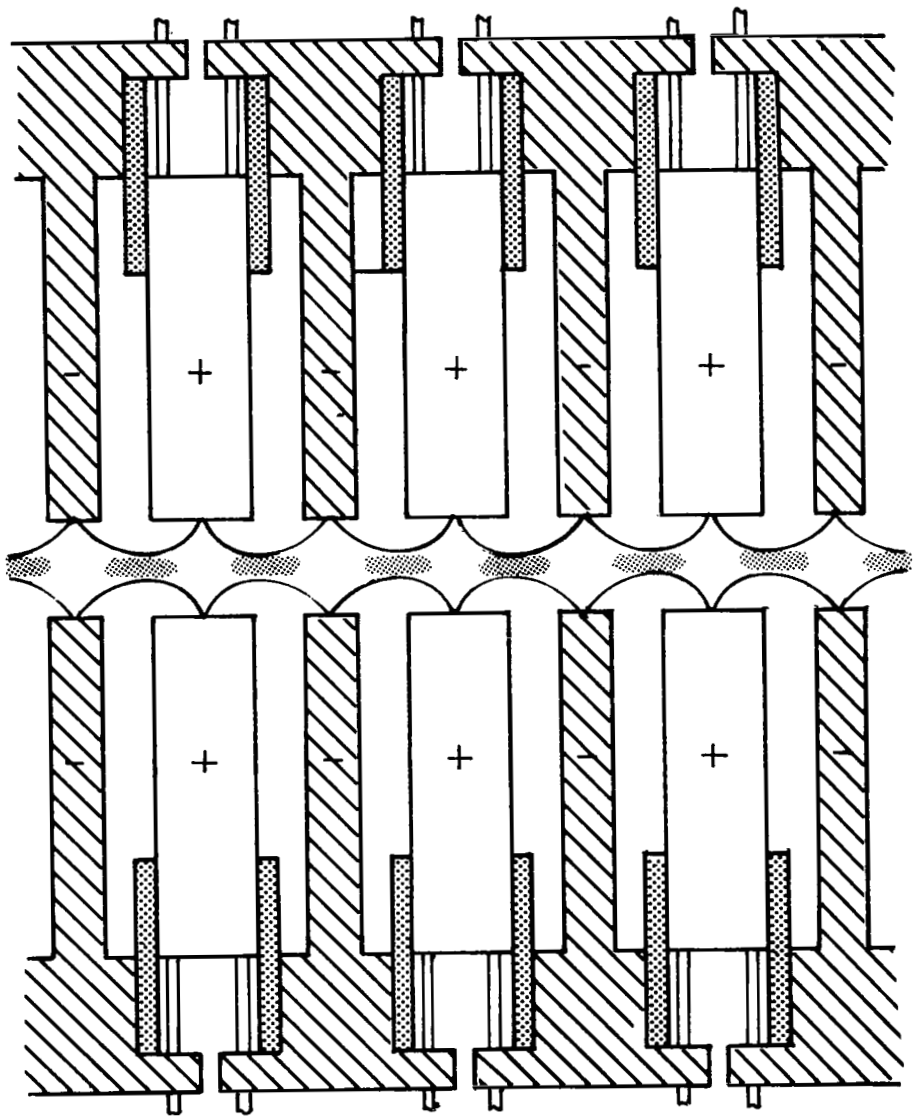

Figure 20.- Multiple arrays of hypocycloidal-pinch devices.

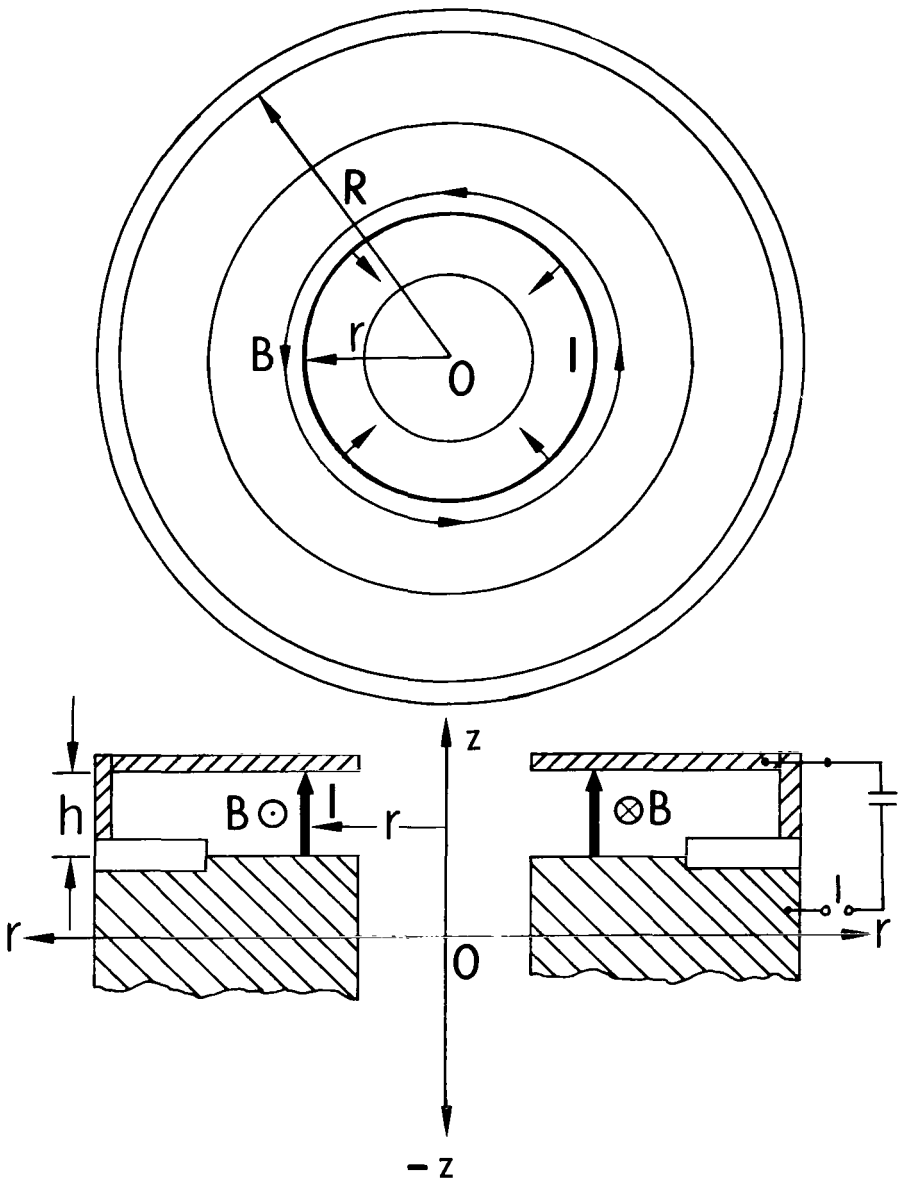

Figure 21.- A snowplow model for current shell in hypocycloidal-pinch apparatus.

NATIONAL AERONAUTICS AND SPACE ADMINISTRATION
WASHINGTON, D.C. 20546

OFFICIAL BUSINESS
PENALTY FOR PRIVATE USE $300

SPECIAL FOURTH-CLASS RATE BOOK

POSTAGE AND FEES PAID
NATIONAL AERONAUTICS AND SPACE ADMINISTRATION
451

U.S.MAIL

156 001 C1 U H 751219 S00903DS
DEPT OF THE AIR FORCE
AF WEAPONS LABORATORY
ATTN: TECHNICAL LIBRARY (SUL)
KIRTLAND AFB NM 87117

156 002 C1 U [illegible] 751219 [illegible]

POSTMASTER : If Undeliverable (Section 158 Postal Manual) Do Not Return

"The aeronautical and space activities of the United States shall be conducted so as to contribute . . . to the expansion of human knowledge of phenomena in the atmosphere and space. The Administration shall provide for the widest practicable and appropriate dissemination of information concerning its activities and the results thereof."

—NATIONAL AERONAUTICS AND SPACE ACT OF 1958

NASA SCIENTIFIC AND TECHNICAL PUBLICATIONS

TECHNICAL REPORTS: Scientific and technical information considered important, complete, and a lasting contribution to existing knowledge.

TECHNICAL NOTES: Information less broad in scope but nevertheless of importance as a contribution to existing knowledge.

TECHNICAL MEMORANDUMS: Information receiving limited distribution because of preliminary data, security classification, or other reasons. Also includes conference proceedings with either limited or unlimited distribution.

CONTRACTOR REPORTS: Scientific and technical information generated under a NASA contract or grant and considered an important contribution to existing knowledge.

TECHNICAL TRANSLATIONS: Information published in a foreign language considered to merit NASA distribution in English.

SPECIAL PUBLICATIONS: Information derived from or of value to NASA activities. Publications include final reports of major projects, monographs, data compilations, handbooks, sourcebooks, and special bibliographies.

TECHNOLOGY UTILIZATION PUBLICATIONS: Information on technology used by NASA that may be of particular interest in commercial and other non-aerospace applications. Publications include Tech Briefs, Technology Utilization Reports and Technology Surveys.

Details on the availability of these publications may be obtained from:

SCIENTIFIC AND TECHNICAL INFORMATION OFFICE

NATIONAL AERONAUTICS AND SPACE ADMINISTRATION

Washington, D.C. 20546